Redox Biology 11 (2017) 438–455

Contents lists available at ScienceDirect

Redox Biology

journal homepage: www.elsevier.com/locate/redox

Research paper

Cross-talk between lipid and protein carbonylation in a dynamic cardiomyocyte model of mild nitroxidative stress

Eva Griesser[a,b], Venukumar Vemula[a,b], Nora Raulien[c], Ulf Wagner[c], Sandra Reeg[d], Tilman Grune[d,e,f], Maria Fedorova[a,b,*]

[a] Institute of Bioanalytical Chemistry, Faculty of Chemistry and Mineralogy, University of Leipzig, Deutscher Platz 5, 04103 Leipzig, Germany
[b] Center for Biotechnology and Biomedicine, University of Leipzig, Deutscher Platz 5, 04103 Leipzig, Germany
[c] Rheumatology Unit, Department of Internal Medicine, University of Leipzig, Liebigstr. 20, 04103 Leipzig, Germany
[d] Department of Molecular Toxicology, German Institute of Human Nutrition, Potsdam-Rehbruecke, Germany
[e] German Center for Diabetes Research (DZD), 85764 München-Neuherberg, Germany
[f] German Center for Cardiovascular Research (DZHK), 10117 Berlin, Germany

ARTICLE INFO

Keywords:
Nitroxidative stress
Cardiomyocytes
Lipid oxidation
Protein oxidation
Lipid-protein adducts
Carbonylation

ABSTRACT

Reactive oxygen and nitrogen species (ROS/RNS) play an important role in the regulation of cardiac function. Increase in ROS/RNS concentration results in lipid and protein oxidation and is often associated with onset and/or progression of many cardiovascular disorders. However, interplay between lipid and protein modifications has not been simultaneously studied in detail so far. Biomolecule carbonylation is one of the most common biomarkers of oxidative stress. Using a dynamic model of nitroxidative stress we demonstrated rapid changes in biomolecule carbonylation in rat cardiomyocytes. Levels of carbonylated species increased as early as 15 min upon treatment with the peroxynitrite donor, 3-morpholinosydnonimine (SIN-1), and decreased to values close to control after 16 h. Total (lipids+proteins) vs. protein-specific carbonylation showed different dynamics, with a significant increase in protein-bound carbonyls at later time points. Treatment with SIN-1 in combination with inhibitors of proteasomal and autophagy/lysosomal degradation pathways allowed confirmation of a significant role of the proteasome in the degradation of carbonylated proteins, whereas lipid carbonylation increased in the presence of autophagy/lysosomal inhibitors. Electrophilic aldehydes and ketones formed by lipid peroxidation were identified and relatively quantified using LC-MS/MS. Molecular identity of reactive species was used for data-driven analysis of their protein targets. Combination of different enrichment strategies with LC-MS/MS analysis allowed identification of more than 167 unique proteins with 332 sites modified by electrophilic lipid peroxidation products. Gene ontology analysis of modified proteins demonstrated enrichment of several functional categories including proteins involved in cytoskeleton, extracellular matrix, ion channels and their regulation. Using calcium mobilization assays, the effect of nitroxidative stress on the activity of several ion channels was further confirmed.

1. Introduction

ROS and RNS at physiological levels play an important role in signaling processes and the regulation of cardiovascular homeostasis [1]. However, overproduction and/or defective elimination of these reactive species leads to the condition known as "oxidative stress" (OS), resulting in modifications of proteins, lipids, carbohydrates and DNA followed by impairment of their functions, accumulation of oxidized

Abbreviations: ROS, reactive oxygen species; RNS, reactive nitrogen species; OS, oxidative stress; CVDs, cardiovascular diseases; HF, heart failure; IR, ischaemia/reperfusion; CM, cardiomyocytes; SIN-1, 3-morpholinosydnonimine; oxoLPPs, carbonylated lipid peroxidation products; DMEM/F12, Dulbecco's Modified Eagle Medium/Ham's F-12; 7-AAD, 7-aminoactinomycin; DCFDA, 2′,7′-dichlorofluorescin diacetate; CHH, 7-(diethylamino)-coumarin-3-carbohydrazide; PFA, paraformaldehyde; TCE, 2,2,2-trichlorethanol; DNPH, 2,4-dinitrophenyl hydrazine; MTBE, *tert*-butyl methyl ether; AMC, 7-amino-4-methylcoumarin; DTT, dithiothreitol; pepA, pepstatin A; IAA, iodoacetamide; HRP, horse radish peroxidase; ARP, aldehyde reactive probe; BSO, buthionine sulfoximine; 8OHQ, 8-hydroxyquinoline; POPA, 1-palmitoyl-2-oleoyl-*sn*-glycero-3-phosphate; DMF, N,N-dimethylformamide; LC3, light chain protein 3; LDH, lactate dehydrogenase; TPBS, Tween-PBS; DDA, data-dependent acquisition; Cu8OHQ, Copper(II)8-hydroxyquinoline complex; oxPC, oxidized phosphatidylcholine; LDs, lipid droplets; HNE, hydroxyl-nonenal; MDA, malondialdehyde; PTMs, post-translational modifications; HHE, hydroxyl-hexenal; LOX, lysyl oxidase; MCO, metal-catalysed oxidation; ECM, extracellular matrix; MyBP-C, myosin binding protein; VDCC, voltage-dependent calcium channel; RyR, ryanodine receptor; IP3R, inositol-1,4,5-trisphosphate receptor

* Correspondence to: Institut für Bioanalytische Chemie, Biotechnologisch-Biomedizinisches Zentrum, Deutscher Platz 5, 04103 Leipzig, Germany.
E-mail address: maria.fedorova@bbz.uni-leipzig.de (M. Fedorova).

http://dx.doi.org/10.1016/j.redox.2016.12.028
Received 23 December 2016; Accepted 27 December 2016
Available online 28 December 2016
2213-2317/

molecules and eventually cell death [2]. OS has been linked to the pathophysiology of numerous cardiovascular diseases (CVDs), including heart failure (HF), cardiomyopathy, myocardium infarction, cardiac hypertrophy, ischaemia/reperfusion (IR) injury and atherosclerosis [3]. Myocardial homeostasis and cardiomyocyte (CM) contraction are tightly regulated via different pathways, among which bioavailability of nitric oxide ($^{\bullet}NO$) was shown to play a significant role [1,4]. However, under OS conditions $^{\bullet}NO$ reacts with superoxide anion ($O_2^{\bullet-}$) resulting in the formation of peroxynitrite ($ONOO^-$). At low levels peroxynitrite modulates various intracellular signaling pathways, but elevated concentrations exert cytotoxic effects [5]. It is a highly reactive molecule that can decompose to other reactive species, including $^{\bullet}OH$ and $^{\bullet}NO_2$, which all together lead to complex nitroxidative stress in the myocardium [6,7]. Peroxynitrite production is significantly increased in various CVDs including myocardial IR [8,9], HF [10,11], atherosclerosis [12] and diabetes [13]. Furthermore, numerous experimental results demonstrate a critical role of peroxynitrite in the pathogenesis of CVDs, including HF and IR injury. Thus, the application of a peroxynitrite decomposition catalyst in a doxorubicin-induced HF model allowed preservation of most cardiac functions and prevented elevated levels of 3-nitrotyrosine and malondialdehyde characteristic for HF [14]. Peroxynitrite donor SIN-1 was shown to induce changes in myocytes electrophysiology similar to those in HF, including changes in action potentials and Ca^{2+} cycling [15].

Increase in lipid and protein oxidation was identified as a major reason of $ONOO^-$ cytotoxicity [16,17]. Upon nitroxidative stress cellular lipids and proteins undergo a variety of oxidative reactions leading to their functional and structural alteration, among which biomolecule carbonylation, e.g. introduction of aldehyde or keto functional groups, showed a positive correlation with the development of numerous human disorders [18,19]. Thus, lipid peroxidation results in a variety of products among which carbonylated (electrophilic) species formed via oxidative cleavage of polyunsaturated fatty acids can further react with nucleophilic groups on other biomolecules including Lys-, Cys-, His- and Arg- amino acid residues in proteins [20,21]. Such lipid-protein adducts often retain the carbonyl functional group (carbonylated proteins) and have been shown to play an important role in OS-related disorders by inducing functional alteration, impairing signaling events and possessing pro-inflammatory properties [22,23].

In contrast to many other oxidative post-translational modifications, biomolecule carbonylation is known to be irreversible [24,25]. Therefore, carbonylated proteins and lipids have to be degraded or metabolized to less reactive species via various detoxification pathways. Several enzymes including glutathione S-transferase, aldehyde dehydrogenase/cytochrome P450 and aldo-keto reductase can detoxify electrophilic aldehydes via conjugation with glutathione, oxidation or reduction [26]. Indeed, glutathione-S-transferase [27] and aldehyde dehydrogenase [28,29] have been shown to play cardio-protective roles in IR injury and cardiomyopathy. Carbonylated proteins are usually degraded by the proteasome (mainly by the ATP- and ubiquitin-independent 20S proteasome), mitochondrial Lon-protease and autophagy/lysosomal pathway. A cardio-protective role of these degradation mechanisms was shown in postischemic heart [30,31].

Despite numerous data on the role of lipid and protein oxidative modifications as well as lipid-protein adducts in the development of various CVDs [23,32], no systematic evaluation of these effects has been performed to date. Here we designed a dynamic model of nitroxidative stress using rat primary cardiomyocytes treated with SIN-1 to evaluate cellular response to sub-toxic levels of peroxynitrite. We assessed the dynamics of biomolecule carbonylation using a combination of fluorescence microscopy and biochemical assays. Furthermore, detailed mass spectrometry based analysis allowed targeting of electrophilic lipid peroxidation products (oxoLPPs) capable of modifying nucleophilic substrates and to utilize this knowledge for data-driven identification of protein targets. Systems biology evaluation of oxoLPP-modified proteins allowed identification of affected cellular pathways which were further confirmed in biochemical tests.

2. Materials and methods

2.1. Materials

Dulbecco's Modified Eagle Medium/Ham's F-12 (DMEM/F12), phosphate buffered saline (PBS), fetal bovine serum (FBS), penicillin-streptomycin, L-glutamine, non-essential amino acids, sodium pyruvate, gelatin and 7-aminoactinomycin D (7-AAD) were obtained from Life Technologies GmbH (Darmstadt, Germany). Horse serum, trypsin-EDTA solution, 2′,7′-dichlorofluorescin diacetate (DCFDA), thiazolyl blue tetrazolium bromide (MTT), β-nicotinamide adenine dinucleotide reduced (NADH), triton-X-100, DMSO, crystal violet solution (aqueous), 7-(diethylamino)-coumarin-3-carbohydrazide (CHH), paraformaldehyde (PFA), Nile Red, Hoechst 33258, thiourea, ß-mercaptoethanol, 2,2,2-trichlorethanol (TCE), hydrochloric acid, 2,4-dinitrophenyl hydrazine (DNPH), primary goat anti-DNP antibody, adenosine 5′-triphosphate (ATP), D-biotin, *tert*-butyl methyl ether (MTBE), formic acid, 4-chloro-3-methylphenol, copper (II) sulfate and all ammonium, magnesium, potassium and sodium salts were purchased from Sigma-Aldrich GmbH (Taufkirchen, Germany). 3-Morpholinosydnonimine (SIN-1), 7-amino-4-methylcoumarin (AMC), *N*-succinyl-Leu-Leu-Val-Tyr-AMC (suc-LLVY-AMC), E64d and MG132 were purchased from Enzo Life Sciences GmbH (Lörrach, Germany). Methanol, ethanol, urea, SDS, glycerol, sucrose and dithiothreitol (DTT) were obtained from Carl Roth GmbH + Co. KG (Karlsruhe, Germany). CHAPS, trypsin, glycine, bovine serum albumin (BSA), pepstatin A (pepA), Coomassie® Brilliant Blue G-250 and Tween® 20 were purchased from Serva Electrophoresis GmbH (Heidelberg, Germany). Iodoacetamide (IAA), Tris, HEPES and EDTA were purchased from Applichem GmbH (Darmstadt, Germany). Low fluorescence PVDF membranes, protein free blocking solution (AdvanBlock™), washing solution (AdvanWash™) and WesternBright™ Sirius HRP substrate were obtained from Advansta Inc. (Biozym Scientific GmbH, Hessisch Oldendorf, Germany). Peroxidase-conjugated donkey anti-goat antibody was from Jackson ImmunoResearch Laboratories, Inc. (West Grove, PA, USA). *N*-(Aminooxyacetyl)-*N*′-biotinyl-hydrazine (aldehyde reactive probe, ARP) was purchased from Dojindo EU GmbH (München, Germany), buthionine sulfoximine (BSO) from Cayman Chemical Company (Biomol GmbH, Hamburg, Germany) and 8-hydroxyquinoline hemisulfate salt hemihydrate (8OHQ) and peroxidase-conjugated goat anti-mouse antibody from Santa Cruz Biotechnology, Inc. (Heidelberg, Germany). Acetonitrile (LC-MS grade) was purchased from VWR International GmbH (Darmstadt, Germany), 1-palmitoyl-2-oleoyl-*sn*-glycero-3-phosphate (sodium salt; POPA) and mouse E06 mAb-TopFluor® from Avanti Polar Lipids, Inc. (Otto Nordwald GmbH, Hamburg, Germany) and Pierce™ monomeric avidin agarose from Thermo Scientific (Perbio Science Deutschland GmbH, Bonn, Germany). *N,N*-dimethylformamide (DMF) was obtained from Biosolve BV (Valkenswaard, Netherlands) and chloroform from Merck KGaA (Darmstadt, Germany). Mouse monoclonal anti-LC3 antibody (APG8, Clone 166AT1234) was obtained from Abgent (San Diego, CA, USA).

2.2. Cell culture

Primary rat cardiomyocytes (Innoprot, Elexalde Derio, Spain) were cultured on gelatin-coated 75 cm^2 flasks or 96-well-plates (CELLSTAR®, Greiner Bio-One GmbH, Frickenhausen, Germany) in DMEM/F12 medium supplemented with 20% FBS, 5% horse serum, 2 mmol/L L-glutamine, 3 mmol/L sodium pyruvate, 0.1 mmol/L non-essential amino acids, 100 U/mL penicillin and 100 µg/mL streptomycin at 37 °C (humidified atmosphere of 5% CO_2 and 95% air). When cells reached 80% confluence and 24 h before treatment medium was

replaced by serum-free medium (DMEM/F12 supplemented with 100 U/mL penicillin and 100 µg/mL streptomycin). Cells were treated with 10 µmol/L SIN-1 for 15 min, 30 min, 70 min and 16 h.

2.3. DCFDA assay

Cardiomyocytes (CM; 20,000 cells per well) were seeded on black flat bottom 96-well-plates. The next day and 24 h before the experiment medium was changed to serum-free medium. Cells were washed with PBS and loaded with 10 µmol/L DCFDA (1 h, 37 °C). After incubation cells were washed (PBS), incubated with PBS (1 h, 37 °C) and treated with SIN-1 (10 µmol/L in PBS). Fluorescence (Ex=485 nm, Em=535 nm) was recorded every 3 min for 16 h at 37 °C using Paradigm™ Detection Platform (Beckman Coulter GmbH, Krefeld, Germany).

2.4. MTT assay

CM (20,000 cells per well) were grown on 96-well-plates. After treatment with 10 µmol/L SIN-1 medium was changed to 1.2 mmol/L MTT in transparent DMEM/F12 (4 h, 37 °C). After incubation SDS (up to 5% w/v) was added and incubated overnight (37 °C). Absorbance was measured at 562 nm (reference 690 nm) with a Sunrise™ microplate reader (Tecan Deutschland GmbH, Crailsheim, Germany).

2.5. Lactate dehydrogenase (LDH) assay

CM (20,000 cells per well) were seeded on 96-well-plates. After SIN-1 treatment (100 µL), 25 µL of the medium was transferred into a new 96-well-plate. 175 µL of LDH solution (0.24 mmol/L NADH, 0.57 mmol/L sodium pyruvate, 33 mmol/L KH_2PO_4, 66 mmol/L K_2HPO_4, pH 7.4) was added and absorbance was recorded at 340 nm every 3 min for 30 min using SpectraMax® Paradigm® Multi-Mode Detection Platform (Molecular Devices GmbH, Biberach an der Riss, Germany). 0.1% Triton-X-100 was used as a positive control for maximum LDH-release and untreated cells as a control for a spontaneous LDH-release.

2.6. CHH labeling and fluorescence microscopy of carbonylated biomolecules [33]

CM (15,000 cells per well) were grown on gelatin-coated cover slips in a 24-well-plate. After SIN-1 treatment cells were washed with PBS (two times), fixed with PFA (4% w/v in PBS, 15 min, 37 °C) and washed again with PBS (three times). Cells were labelled with CHH (0.2 mmol/L, 2 h, RT) and washed with 0.1% Tween in PBS (TPBS, three times). Nuclei were counterstained with 7-AAD (1:300 in 0.1% TPBS, 30 min, RT) followed by washing (two times with TPBS, one time PBS). Cover slips were mounted on cover slides using Immunoselect Antifading Mounting Medium (Dianova GmbH, Hamburg, Germany). Cells were examined by inverted fluorescence microscope (DMI6000B, Leica Mikrosysteme Vertrieb GmbH, Wetzlar, Germany), equipped with 10x (NA 0.25), 20x (NA 0.40) and 40x objectives (NA 0.60), a 12V/100W halogen lamp as light source and a Leica DFC360FX camera. Images of 7-AAD were acquired with a filter cube TRI (Ex: R, bandpass (BP) 575/20 nm, Em: longpass (LP) 580 nm) and CHH with filter cube TRI (Ex: B, BP 387/11 nm, Em: BP 535/40 nm). For acquisition of images Leica Application Suite (LAS AF) microscope software (version 2.3.0) was used. Images were quantified using ImageJ software [34].

Alternatively, CM (7,000 cells per well) were seeded on 96-well-plates and next day treated with SIN-1 in the absence or presence of inhibitors (MG132 [20 µmol/L], E64d and pepstatin A [5 µg/mL both], buthionine sulfoximine [500 µmol/L], 8-hydroxyquinoline and $CuSO_4$ [2.5 µmol/L both]) or with inhibitors alone. After treatment cells were washed, fixed with PFA and labelled with CHH as described above. Images were acquired by fluorescence microscopy and quantified using ImageJ. Quantification results were normalized to cell numbers obtained by crystal violet staining [35]. For that PFA-fixed cells were stained with aqueous crystal violet (0.1% , 20 min, RT), washed with water (3 times), dissolved in ethanol (70%, 1 h, RT), and absorbance was measured at 590 nm using SpectraMax® Paradigm® Multi-Mode Detection Platform (Molecular Devices).

2.7. Protein extraction

After SIN-1 treatment cells were scraped into ice cold PBS and collected by centrifugation (10 min, 10001000×*g*, 4 °C). Cell pellets were washed with ice cold PBS (two times) and resuspended in lysis buffer (7 mol/L urea, 2 mol/L thiourea, 2% CHAPS in 50 mmol/L Tris-HCl, pH 7.5). Samples were sonicated on ice using a Vibra-Cell™ tip sonicator (20 kHz, 1 min with on/off pulse 5 s each, 40% amplitude; Sonics & Materials, Inc., Newtown, CT, USA) followed by centrifugation (20 min, 10,00010,000×*g*, 4 °C). Supernatants were collected and protein concentration was determined by Bradford assay [36].

2.8. Western Blot analysis of carbonylated proteins (Oxyblot)

Proteins in lysis buffer (10 µg) were mixed with Laemmli sample buffer (62.5 mmol/L Tris-HCl pH 6.8, 20% v/v glycerol, 2% w/v SDS, 5% v/v ß-mercaptoethanol, 0.01% w/v bromophenol blue) and separated by SDS-PAGE (10% T, 0.75 mm, containing 0.5% (v/v) TCE, 200 V; BioRad mini protean III cell; BioRad Laboratories GmbH, München, Germany). TCE in-gel visualization was performed as described before [37]. Briefly, TCE containing gels were exposed to UV light for 1 min and the fluorescence of TCE-UV-modified tryptophan residues in proteins was visualized to confirm equal loadings of the samples. Proteins were tank blotted onto a low-fluorescence PVDF membrane in Bjerrum Schafer-Nielsen transfer buffer (48 mmol/L Tris, 39 mmol/L glycine) using Mini Trans-Blot® Cell (60 min, 100 V; BioRad). After blotting DNPH derivatization of carbonylated proteins was performed as described before [38] with slight modifications. Briefly, membranes were incubated in 2 mol/L HCl (10 min), derivatized with DNPH (1 mg/mL in 2 mol/L HCl; 30 min) and washed with 2 mol/L HCl (10 min) and methanol (5 min; five times). Membranes were blocked overnight (4 °C, protein free blocking solution), incubated with primary goat anti-DNP antibody (1 h, 1:10,000 in blocking solution, RT) and washed (10 min, three times, washing solution). Afterwards membranes were incubated with peroxidase-conjugated donkey anti-goat antibody (1 h, 1:10,000 in blocking solution, RT) followed by washes with washing solution (10 min; two times) and Tris-buffered saline (TBS, 20 mmol/L Tris, 500 mmol/L NaCl; 10 min). Membranes were developed with enhanced chemiluminescence (ECL) using WesternBright™ Sirius HRP substrate. Images were taken with the Fusion FX7 imaging system (Peqlab Biotechnologie GmbH, VWR International GmbH, Erlangen, Germany). Images were quantified using ImageJ by measuring the intensity of the whole protein lane.

2.9. Western Blot analysis of LC3-I/LC3-II proteins

Pellets from SIN-1 treated cells ($2x10^6$ cells) were dissolved in Laemmli sample buffer (62.5 mmol/L Tris-HCl, pH 6.8, 50 mmol/L DTT, 2% w/v SDS, 20% v/v glycerol, 0.2% w/v bromophenol blue), sonicated (8 s, 30% amplitude) and boiled (5 min, 95 °C). Proteins were separated by SDS-PAGE (15%-Tris-Tricine-Gel; BioRad) and blotted onto a PVDF membrane (0.2 µm GE Healthcare, Buckinghamshire, England; Trans-Blot® Cell, BioRad). Membranes were blocked overnight (4 °C, 5% dry milk in TPBS), incubated with primary mouse monoclonal anti-LC3 antibody (3 h, 1:250 in blocking buffer, RT) and washed (TPBS). Peroxidase-conjugated goat anti-mouse antibody (1 h, 1:10,000 in blocking buffer, RT) was added. Membranes were washed and developed using Western Lightning Plus

(Perkin Elmer, Waltham, USA) and Lucent Blue X-ray film (Advansta, Menlo Park, CA, USA). Images were quantified using ImageJ.

2.10. Measurement of the proteasomal chymotrypsin-like activity

Following SIN-1 treatment cell pellets were collected as described before [39]. Cells were lysed with ice cold lysis buffer (250 mmol/L saccharose, 25 mmol/L HEPES, 10 mmol/L $MgCl_2x6H_2O$, 1 mmol/L EDTA, 1.67 mmol/L DTT) and resuspended with a 21 G needle on ice (20 times). Cells were disrupted by four freeze-thaw-cycles and centrifuged (10 min, 00020.000×*g*, 4 °C). Protein concentration of the supernatant was determined by Bradford assay. For the measurement of the proteasome activity black 96-well-plates were used. During the preparation solutions and plates were kept on ice. Protein extract (10 µL), 1 mol/L DTT (0.2 µL), 450 mmol/L Tris buffer pH 8.2 containing 90 mmol/L KCl, 15 mmol/L Mg-acetate and 15 mmol/L $MgCl_2$ (33.3 µL) and water (66.5 µL) were mixed and incubated (10 min, RT). After incubation the fluorigenic peptide suc-LLVY-AMC (2 mmol/L, 10 µL) was added. For ATP-stimulated proteasome activity water volume was reduced to 61.5 µL and 100 mmol/L ATP (5 µL) was added after incubation. Fluorescence (Ex=360, Em=460 nm) of the released AMC was recorded for 90 min at 37 °C with Paradigm™ Detection Platform (Beckman Coulter, Brea, USA). A calibration curve was prepared with free AMC standard to calculate the amount of substrate converted by the proteasome.

2.11. Nile Red staining and fluorescence microscopy of neutral lipids

CM (20,000 cells per well) were grown on 96-well-plates. After SIN-1 treatment cells were washed with PBS (two times), incubated with Nile Red (1:1000, 1 mg/mL in DMSO, 10 min, 37 °C), washed (PBS) and examined with fluorescence microscopy as described above using filter cube TRI (Ex: R, BP 575/20 nm, Em: LP 580 nm).

2.12. Immunocytochemical detection of oxidized phosphatidylcholine lipids

CM (20,000 cells per well) were grown on 96-well-plates. After SIN-1 treatment cells were washed with PBS (two times), fixed with PFA (4% w/v in PBS, 15 min 37 °), washed (PBS) and incubated with blocking solution (1% w/v BSA in PBS, 1 h, RT) followed by incubation with mouse E06-mAb-TopFluor® (1:100 in PBS, 1 h, RT). Cells were washed with PBS (three times) and nuclei were counterstained with Hoechst 33258 (2.5 mg/mL in water, 1:1000, 30 min, RT) followed by washes with PBS (two times). Cells were examined by inverted fluorescence microscope as described above filter cube TRI (Ex: G, BP 494/20 nm, Em: BP 535/40 nm).

2.13. Calcium mobilization assay

Calcium mobilization was monitored using FLUOFORTE® Calcium assay kit for microplates (ENZ-51017; ENZO Life Sciences GmbH, Lörrach, Germany) according to the manufacturer's protocol. Briefly, CM (30,000 cells per well) were grown on black 96-well-plates with transparent bottom. Control and treated cells (10 µmol/L SIN-1, 70 min) were washed with PBS, incubated with a dye solution (100 µL, 60 min, RT), calcium channel agonists were added at different concentrations (ATP and 4-chloro-3-methylphenol in Hank's balanced salt solution; POPA in 3 mmol/L NH_4HCO_3) and fluorescence (Ex=490 nm, Em=525 nm) was recorded with 3 readings per well every 2 s for 110 s with a FlexStation 3 Multi-Mode Microplate Reader (Molecular Devices, Sunnyvale, CA, USA).

2.14. CHH labeling and mass spectrometry analysis of carbonylated lipids [40–42]

Cell pellets were resuspended in 0.1% aqueous ammonium acetate (w/v, 50 µL) and derivatized with CHH (3.5 µL, 100 mmol/L in DMF, 1 h, 37 °C). Lipids were extracted using methyl-tert-butylether (MTBE) as described previously [43]. A nano-Acquity UPLC (Waters GmbH, Eschborn, Germany) was coupled online to a LTQ Orbitrap XL ETD mass spectrometer equipped with a nano-ESI source (Thermo Fischer Scientific, Bremen, Germany) operating in positive ion mode. Eluent A was aqueous formic acid (0.1% v/v), and eluent B was formic acid (0.1% v/v) in acetonitrile. CHH-derivatized lipids (10 µL in 30% aqueous acetonitrile) were loaded onto the trap column (nanoAcquity BEH 300 C4, internal diameter 180 µm, length 20 mm, particle diameter 1.7 µm) at a flow rate of 5 µL/min. Lipids were separated on a BEH300 column (C4-phase, internal diameter 100 µm, length 100 mm, particle diameter 1.7 µm) with a flow rate of 0.8 µL/min using linear gradients from 30% to 90% of eluent B (10 min), and holding this composition for 7 min. The transfer capillary temperature was set to 200 °C and tube lens voltage to 110 V. An ion spray voltage of 1.5 kV was applied to a PicoTip™ on-line nano-ESI emitter (New Objective, Berlin, Germany). The precursor ion survey scans were acquired at an Orbitrap (resolution of 100,000 at m/z 400) for a m/z range from 320 to 1500. The CID-tandem mass spectra (isolation width 2 *m/z* units, activation Q 0.25, normalized collision energy 25%, activation time 30 ms) were recorded by data-dependent acquisition (DDA) for the top 6 most abundant ions in each survey scan with dynamic exclusion for 60 s using Xcalibur software (version 2.0.7).

CHH-derivatized oxoLPPs were manually identified based on their CID fragment spectra. To determine the range of the instrument linear response for identified CHH-oxoLPPs each sample was analysed by LC-MS in three dilutions (1:1, 1:2 and 1:4). Only signals showing linear response for all dilution points were considered for quantification. Identified CHH-oxoLPPs were relatively quantified by integrating the area under the curve for corresponding XICs ($m/z \pm 0.01$) at specific retention times (± 20 s) using LCquan™ version 2.5 (Thermo Fisher Scientific) within the Xcalibur software. The average peak width for CHH-oxoLPP adducts was around 25–45 s (Fig. S1), signal-to-noise ratio for detection and quantification were set to three and ten, respectively. The average of peak areas for the control sample (three dilutions each measured in three replicates) was normalized to 100% for each CHH-oxoLPP adduct. Averaged peak areas of corresponding CHH-oxoLPP signals in other samples were expressed relative to control.

2.15. In-solution tryptic digestion and ARP derivatization of carbonylated proteins [44]

Proteins (100 µg) in lysis buffer were reduced with DTT (50 mmol/L, 90 min, 37 °C, 350 rpm) and free thiols were alkylated with IAA (15 mmol/L, 60 min, 27 °C, 350 rpm, in the dark). Samples were diluted with 50 mmol/L NH_4HCO_3 to a final concentration of 1 mol/L urea and digested with trypsin overnight (1:50 trypsin to protein ratio, in 3 mmol/L NH_4HCO_3, 37 °C, 350 rpm). Samples were desalted by solid-phase extraction using Waters Oasis HLB 1cc (10 mg). The stationary phase was rinsed with methanol (1 mL) and equilibrated with water (1 mL). Samples were loaded, washed (0.1% formic acid in 7% aqueous acetonitrile; 1 mL, three times) and peptides were eluted with 0.5% formic acid in 70% aqueous acetonitrile (500 µL). Eluates were vacuum concentrated, dissolved in 1% formic acid in 7% aqueous acetonitrile and labelled with 10 mmol/L ARP (2 h, 27 °C, 550 rpm). Excess of ARP was removed by solid-phase extraction as described above.

2.16. Enrichment of ARP-labelled peptides by avidin affinity chromatography

Affinity enrichment was performed as described recently [44]. Pierce monomeric avidin agarose (100 µL) was packed in mini-spin columns with Luer-lok adapter (Thermo Scientific, Bonn, Germany) and washed with 10 mmol/L NaH_2PO4 (pH 7.4, 1.5 mL). Irreversible binding sites were blocked with D-biotin (2 mmol/L, 300 µL), resin was washed with glycine-HCl (0.1 mmol/L, pH 2.8, 500 µL) and equilibrated with PBS (20 mmol/L NaH_2PO4, 0.3 mol/L NaCl, pH 7.4, 2 mL). ARP-labelled samples in PBS were loaded, incubated for 15 min, washed with PBS (1 mL), 10 mmol/L NaH_2PO4 (pH 7.4, 1 mL), ammonium bicarbonate (50 mmol/L in 20% methanol; 2 mL) and water (1 mL) before the peptides were eluted (500 µL, 0.4% formic acid in 30% aqueous acetonitrile). Peptides were vacuum concentrated and stored at −20 °C. Shortly before MS analysis the samples were dissolved in 25 µL of 0.1% formic acid in 3% aqueous acetonitrile and further diluted 1:5.

2.17. In-gel tryptic digestion for analysis of Schiff-base modified proteins

Proteins (15 µg) were separated by SDS-PAGE (12% T, 1 mm) and stained with Coomassie Brilliant Blue G-250. Protein lanes were cut into five equal slices. Each slice was destained with 50% (v/v) acetonitrile in 50 mmol/L NH_4HCO_3 (1 h, 37 °C, 750 rpm), dehydrated with 100% acetonitrile and dried by vacuum concentration. Proteins were digested with trypsin in 3 mmol/L NH_4HCO_3 (375 ng, 4 h, 37 °C, 550 rpm) and peptides were extracted using consecutive incubations with 100%, 50% and 100% acetonitrile (15 min sonication for each step). Combined extracts were vacuum concentrated and stored at −20 °C. Before MS analysis peptides were dissolved in 10 µL of 0.5% formic acid in 60% aqueous acetonitrile and further diluted 1:20 with 0.1% formic acid in 3% aqueous acetonitrile.

2.18. LC-MS/MS of tryptic peptides

A nano-Acquity UPLC (Waters GmbH, Eschborn, Germany) was coupled online to an LTQ Orbitrap XL ETD mass spectrometer equipped with a nano-ESI source (Thermo Fischer Scientific, Bremen, Germany). Eluent A was aqueous formic acid (0.1% v/v), and eluent B was formic acid (0.1% v/v) in acetonitrile. Samples (10 µL; in three biological replicates) were loaded onto the trap column (nanoAcquity symmetry C18, internal diameter 180 µm, length 20 mm, particle diameter 5 µm) at a flow rate of 10 µL/min. Peptides were separated on BEH 130 column (C18-phase, internal diameter 75 µm, length 100 mm, particle diameter 1.7 µm) with a flow rate of 0.4 µL/min. Affinity enriched ARP-labelled peptides were separated using several linear gradients from 3% to 9% (2.1 min), 9.9% (1.9 min), 17.1% (10 min), 18% (0.5 min); 20.7% (0.2 min), 22.5% (3.1 min), 25.6% (3 min), 30.6% (5 min), 37.8% (2.8 min) and finally to 81% eluent B (2 min). Together with an equilibration time of 12 min the samples were injected every 46 min. In-gel digested peptides were separated using two step gradients from 3% to 30% eluent B over 18 min and then to 85% eluent B over 1 min. After an equilibration time of 12 min samples were injected every 33 min. The transfer capillary temperature was set to 200 °C and the tube lens voltage to 120 V. An ion spray voltage of 1.5 kV was applied to a PicoTip online nano-ESI emitter (New Objective, Berlin, Germany). The precursor ion survey scans were acquired at an orbitrap (resolution of 60,000 at *m/z* 400) for a *m/z* range from 400 to 2000. CID-tandem mass spectra (isolation width 2, activation Q 0.25, normalized collision energy 35%, activation time 30 ms) were recorded in the linear ion trap by data-dependent acquisition (DDA) for the top six most abundant ions in each survey scan with dynamic exclusion for 60 s using Xcalibur software (version 2.0.7). For in-gel digested peptides identical LC-MS/MS analysis with both CID and ETD fragmentation (activation time 100 ms, isolation width 2 u) was performed. The first set of LC-MS/MS with ETD fragmentation was used to identify highly abundant unoxidized peptides using Sequest search engine (Proteome Discoverer 1.4, Thermo Scientific) against Uniprot *Rattus norvegicus* database (downloaded on March 11, 2014, entries: 7,889 proteins), allowing up to two missed cleavages and a mass tolerance of 10 ppm for precursor ions and 0.8 Da for product ions. Oxidation of methionine and carbamidomethylation of cysteine were used as variable modifications and results were filtered for rank 1 peptides and score vs. charge states corresponding to Xcorr/z 2.0/2, 2.25/3, 2.5/4, 2.75/5. The list of *m/z* values corresponding to identified peptides was exported and used as exclusion list for the second LC-ETD-MS/MS analysis.

2.19. Database search

The acquired tandem mass spectra were searched against the Uniprot *Rattus norvegicus* database using Sequest search engine (Proteome Discoverer 1.4, Thermo Scientific), allowing up to two missed cleavages and a mass tolerance of 10 ppm for precursor ions and 0.8 Da for product ions. A list of variable modifications used for database search always included oxidation of Met, Cys and Trp, carbamidomethylation (ARP-labelled dataset) or propionamide on Cys (in-gel digestion dataset) and a set of oxoLPP derived modifications based on the molecular weight of electrophilic lipids identified (Table S1). Search results were filtered for rank 1 (ARP labelled samples), high confidence and score vs. charge states corresponding to Xcorr/z 2.0/2, 2.25/3, 2.5/4, 2.75/5 (in-gel digested samples). For both datasets only peptides identified by MS/MS in at least two biological replicates with a corresponding (*m/z* and retention time) precursor ion manually confirmed in the third biological replicate were considered. The resulting set of modified proteins was evaluated using STRING network analysis (version 10.0) [45] and manually annotated based on their gene ontology terms (biological process and molecular function) provided by UniProtKB.

3. Results and discussion

Oxidative stress under (patho)physiological conditions has a complex aetiology and is usually mediated by a variety of reactive species, rather than a single type of ROS or RNS. To study the cross-talk between lipid and protein modifications, a dynamic model of nitroxidative stress based on SIN-1 treatment of rat primary cardiomyocytes (CM) was used [46]. In aqueous solution SIN-1 readily decomposes to nitric oxide ($^{\bullet}NO$) and superoxide anion ($O_2^{\bullet-}$), which in turn form peroxynitrite anion ($ONOO^-$). The peroxynitrite anion exists in equilibrium with its acidic form (ONOOH) and can generate hydroxyl ($^{\bullet}OH$) and nitrogen dioxide ($^{\bullet}NO_2$) radicals as well as nitrate (NO_3^-). In the presence of carbon dioxide (CO_2) peroxynitrite anion forms nitrosoperoxocarbonate ($ONOOCO_2^-$), which in turn decomposes to $^{\bullet}NO_2$, CO_3^- and NO_3^- [47]. We and others have previously demonstrated the complex nitroxidative effect of SIN-1 treatment in cell culture models [46,48–50]. Here, free radical production in SIN-1-treated (10 µmol/L) CM was monitored by DCFDA assay (Fig. S2A) over 16 h. Rapid increase in DCF fluorescence was characteristic for the first hour after SIN-1 addition reaching the maximum at 70 min. The half-life of SIN-1 decomposition in aqueous solution was determined to be 30 min, with complete consumption from 60 to 90 min [49,51], further confirming our results. To design a dynamic model of nitroxidative stress, several time points for SIN-1 cell treatment were selected: 15 min (stress onset), 30 min (development), 70 min (highest radical concentration) and 16 h (regeneration). None of the conditions used for CM incubations were toxic. Cell viability was above 90% of the control level for all experimental time points (Fig. S2B). Similarly, cytotoxicity did not exceed 10% as determined by LDH assay (Fig. S2C).

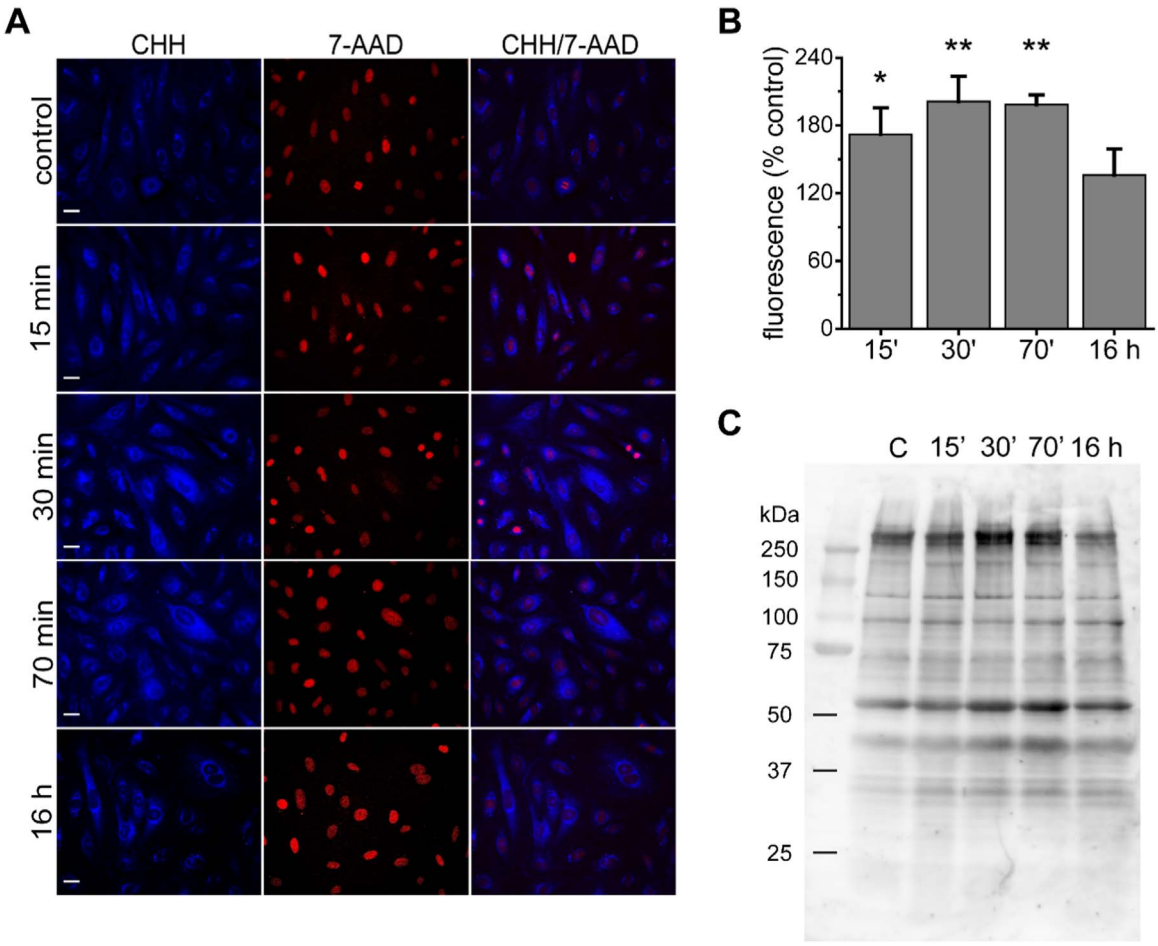

Fig. 1. : Fluorescence microscopy of protein and lipid carbonyls labelled with CHH and oxyblot analysis of protein carbonylation. (A) Primary rat cardiomyocytes were treated with 10 µmol/L SIN-1, fixed with 4% PFA and labelled with 0.5 mmol/L CHH for 2 h. Nuclei were counterstained with 7-AAD for 30 min. Images are representatives of three independent experiments performed in triplicates. Scale bars 20 µm. (B) Carbonylation levels were evaluated by CHH fluorescence microscopy and images were quantified by ImageJ. Data is shown as means ± SE (* $p < 0.05$, ** $p < 0.01$ vs. control) of 15–25 cell images obtained from three independent experiments. (C) Protein carbonylation was analysed using anti-DNP-Western Blot (oxyblot). Image is representative of three independent experiments.

3.1. Cellular carbonylation

Biomolecule carbonylation, e.g. introduction of carbonyl function as a result of oxidative modifications in proteins, lipids and nucleic acids, is a well-known marker of oxidative damage [19,52]. To assess cellular nitroxidative stress upon SIN-1 treatment, total biomolecule carbonylation was monitored using the specific membrane permeable fluorescent probe 7-(diethylamino)-coumarin-3-carbohydrazide (CHH) (Fig. 1A) [33,53]. A significant increase in CHH fluorescence (175%) was observed already 15 min after SIN-1 addition indicating rapid oxidation of biomolecules by ROS/RNS. Maximum intensity (200%) was reached after 30 min and remained at this level until the 70 min time point. Interestingly, CHH fluorescence intensity in CM incubated with SIN-1 for 16 h was close to the control level (120%), indicating efficient removal of modified molecules (Fig. 1B).

Application of microscopy imaging allowed not only the relative quantification of cellular carbonylation but also revealed the spatial distribution of modified biomolecules. In agreement with previous reports [33,54,55], carbonylated species were not equally distributed over the whole cell but displayed strong perinuclear accumulation. Slight accumulation of carbonyl specific fluorescence signal around the cell nucleus was detected even in untreated cells. However, SIN-1 treatment induced a significant increase in perinuclear carbonylation as early as 15 min. Cells treated with SIN-1 for 30 and 70 min displayed the most intense fluorescence signals around the nucleus. This effect was diminished after 16 h of treatment. In addition, cells treated for 30 and 70 min displayed less intense but prominent signals distributed in the cytoplasm resembling filament- and dot-like structures (Fig. 1A).

In contrast to the commonly used immunochemical detection, CHH derivatization not only allows detection of carbonylated proteins but also lipids [33]. Thus, the rapid increase in cellular carbonylation observed 15 min after SIN-1 treatment can be attributed to at least two types of biomolecules. To address protein carbonylation more specifically, a standard oxyblot protocol based on carbonyl derivatization with DNPH followed by immunodetection with anti-DNP antibody, was used (Fig. 1C). In contrast to the fluorescence microscopy data, almost no change in protein-bound carbonyls was detected after 15 min of SIN-1 treatment, whereas samples treated for 30 and 70 min displayed significantly higher levels of carbonylated proteins (Fig. S3). Thus proteins with molecular weight around 45 and 55 kDa showed a time-dependent elevation in protein carbonylation with a maximum after 70 min of SIN-1 treatment relative to the control, while protein bands above 250 kDa showed only a mild increase in protein bound carbonyls. 16 h after stress induction protein carbonylation levels of individual bands showed a mild decrease compared to 30 and 70 min time points. However, the effect was not as strong as shown by the microscopy results.

Our cellular model demonstrated that non-toxic levels of ROS/RNS are capable of rapid induction of biomolecule carbonylation. Indeed, it was reported that 10 µmol/L SIN-1 would correspond to 3 nmol/L of peroxynitrite and thus represent physiological rather than pathological

conditions [48]. Furthermore, the differences in the total (175% increase at 15 min) and protein-specific (significant increase at 30 min) carbonylation suggested that compared to proteins, lipids might be the primary targets of ROS/RNS.

Lipids with polyunsaturated fatty acyl chains are among the first targets of reactive radicals [20]. Lipid oxidation results in a large variety of products, including truncated species formed via oxidative cleavage (e.g. Hock cleavage or β-scission) carrying newly introduced carbonyl functions (keto or/and aldehyde groups). Among the most studied carbonylated lipid peroxidation products (oxoLPPs) are hydroxy- and oxo-nonenal, hydroxy- and oxo-hexenal as well as short chain dicarbonyl compounds such as glyoxal, methylglyoxal and malondialdehyde [20,56–59]. All of these compounds are strong electrophiles capable of reacting with cellular nucleophiles unless they are rapidly detoxified. Thus, nucleophilic protein amino acid residues (Lys, His, Cys and to a lesser extent Arg) can react with oxoLPPs via at least two mechanisms - Schiff base formation and Michael addition. In the case of Schiff base formation the carbonyl functionality is consumed, while protein-oxoLPP Michael adducts still carry the carbonyl group, effectively shifting the carbonyl signal from the lipid to the protein fraction [60].

However, a significant decrease in signal intensity for total carbonylation and a mild decrease for protein specific carbonylation was observed 16 h after SIN-1 addition, indicating efficient removal of the modified species (Fig. 1). Taking into account the high cell viability and post-mitotic nature of CM, the decrease of carbonylation cannot be attributed to the death of affected cells or modification "dilution" through cell divisions. Furthermore, both lipid and protein carbonylation are generally considered as irreversible and cannot be repaired by cellular enzymatic machinery. Thus, carbonylated molecules should be either detoxified or degraded within the cell.

3.2. Carbonylated biomolecule turnover

Removal of modified biomolecules can be achieved via their degradation or conversion to less reactive species. Electrophilic oxoLPPs are metabolized via different reactions catalysed by aldo-keto reductases (reduction), aldehyde dehydrogenase/cytochrome P450 (oxidation) and glutathione S-transferase (conjugation with GSH) [26,61]. Carbonylated proteins can be degraded by the proteasome (mostly by 20S proteasome in ATP and ubiquitin independent manner) and the mitochondrial Lon-protease [62]. Furthermore, the role of autophagy/lysosomal degradation pathway in the removal of oxidized proteins was recently demonstrated [63].

Here we determined the chymotrypsin-like activity of the proteasome with and without ATP-stimulation in SIN-1 treated CM using the fluorogenic peptide suc-LLVY-AMC as a substrate. A significant increase (120%) in the proteasome activity without ATP-stimulation accompanied by a mild decrease (90%) in ATP-stimulated activity occurred 15 min after SIN-1 treatment compared to the control (Fig. 2A). However, at the 30 min time point proteasome activitity returned to control levels. These results indicate that the 20S proteasome, capable of degrading oxidized proteins, was required only in the first few minutes after OS induction. Further protein quality control did not require elevated 20S proteasome activity, indicating that other mechanisms could be involved in the removal of modified species. For instance, autophagy/lysosomal degradation of cellular biomolecules, usually activated in response to nutrient deprivation, was recently reported to be induced by OS [64,65] and to participate in the removal of modified proteins. Furthermore, although oxoLPP-protein adducts are largely believed to be stable, some reports indicate the possibility of retro-Michael addition reaction resulting in decrease of protein carbonylation. Yang et al. recently reported decrease in HNE-protein adducts in RKO cells one and four hours after HNE treatment independent of MG132 treatment using a quantitative LC-MS approach [66].

In order to specify the role of the proteasomal system in the degradation of modified proteins and to identify other possible mechanisms of carbonylated species removal, we quantified CHH specific fluorescence to monitor total biomolecule carbonylation in SIN-1 treated cells in the presence or absence of specific inhibitors of proteasome, autophagy/lysosomal degradation and GSH synthesis.

MG132 and Cu(II)–8-hydroxyquinoline [Cu(8OHQ)] were used to inhibit proteasomal degradation in SIN-1 treated cells (Fig. 2B-C and S4). When SIN-1 treatment was combined with MG132 a significant increase in carbonylation was observed for 70 min and 16 h time points. Visual analysis of fluorescence microscopy images (Fig. S4) showed an accumulation of dot-like structures surrounding the nucleus representing carbonylated lipids and proteins. However, it is important to note that MG132 additionally inhibits calpains and lysosomal cathepsins [67], thus the effect on carbonylation levels can be partially attributed to the inhibition of lysosomal degradation. In contrast to MG132, application of the more selective proteasome inhibitor Cu(8OHQ) [68,69] resulted in elevated carbonylation levels only after 16 h (Fig. 2C).

Inhibition of GSH synthesis using buthionine sulfoximine (BSO) in combination with SIN-1 treatment, did not result in any differences in biomolecule carbonylation compared to SIN-1 treated cells (Fig. 2D). However, it is possible, that the amount of GSH available in the cell is enough for aldehyde conjugation considering the short time intervals used in our model. Intermediate time points (4 and 6 h upon stress induction) might demonstrate significance of GSH synthesis for removal of carbonylated species as it was shown for acrolein treated human bronchiolar epithelial cells [70].

Finally, treatment with E64d and pepstatin A, inhibitors of lysosomal proteases, in the presence of SIN-1 displayed a significant increase in carbonylation levels at 15 min time point in comparison to only SIN-1 treated cells (Fig. 2E). To confirm the role of lysosomal/autophagy degradation pathway in the removal of carbonylated species, we determined the ratio between non-lipidated (LC3-I) and lipidated (LC3-II) forms of protein light chain 3, a common marker for autophagy (Fig. 2F). The results clearly demonstrate significant activation of autophagy degradation pathway already at 15 min after stress induction, reaching its maximum at 70 min of SIN-1 treatment.

Thus, the application of selective inhibitors followed by fluorescence microscopy evaluation of total carbonylation in SIN-1 treated CM allowed demonstration of the importance of at least two independent degradation mechanisms. Autophagy/lysosomal degradation played a critical role at early stages of stress induction, whereas proteasomal degradation of carbonylated proteins was important at the later time points. Taking into account the low level of protein carbonylation (Fig. 1C) in comparison to total carbonyls (Fig. 2A-B) at 15 min time point, the fast increase in carbonyl specific fluorescence in the presence of E64d/pepstatin A was attributed to the accumulation of oxoLPPs.

Induction of autophagy by oxidized lipids had been demonstrated in several studies. Human aortic smooth muscle cells activated autophagy in response to the treatment with 7-ketocholesterol by enhanced formation of hydrogen peroxide via NADPH oxidase (Nox4) [71]. Treatment of ARPE-19 cells (human retinal pigmented epithelium) with methylglyoxal induced accumulation of autophagosomes and phosphorylation of p38 MAPK, JNK1/2, Akt and ERK1/2 [72]. Induction of autophagy by oxidized phospholipids was shown in epidermal keratinocytes exposed to UVA [73]. Hill et al. reported that unsaturated aldehydes such as hydroxy-nonenal (HNE) activate autophagy for degradation of oxoLPP-protein adducts in vascular smooth muscle cells [74]. Treatment of rat aortic smooth muscle cells with HNE induced ER stress and activated JNK leading to autophagy stimulation [75].

3.3. Lipid accumulation and oxidation in the presence of lysosomal/autophagy inhibitors

To further confirm the correlation between increased lipid carbo-

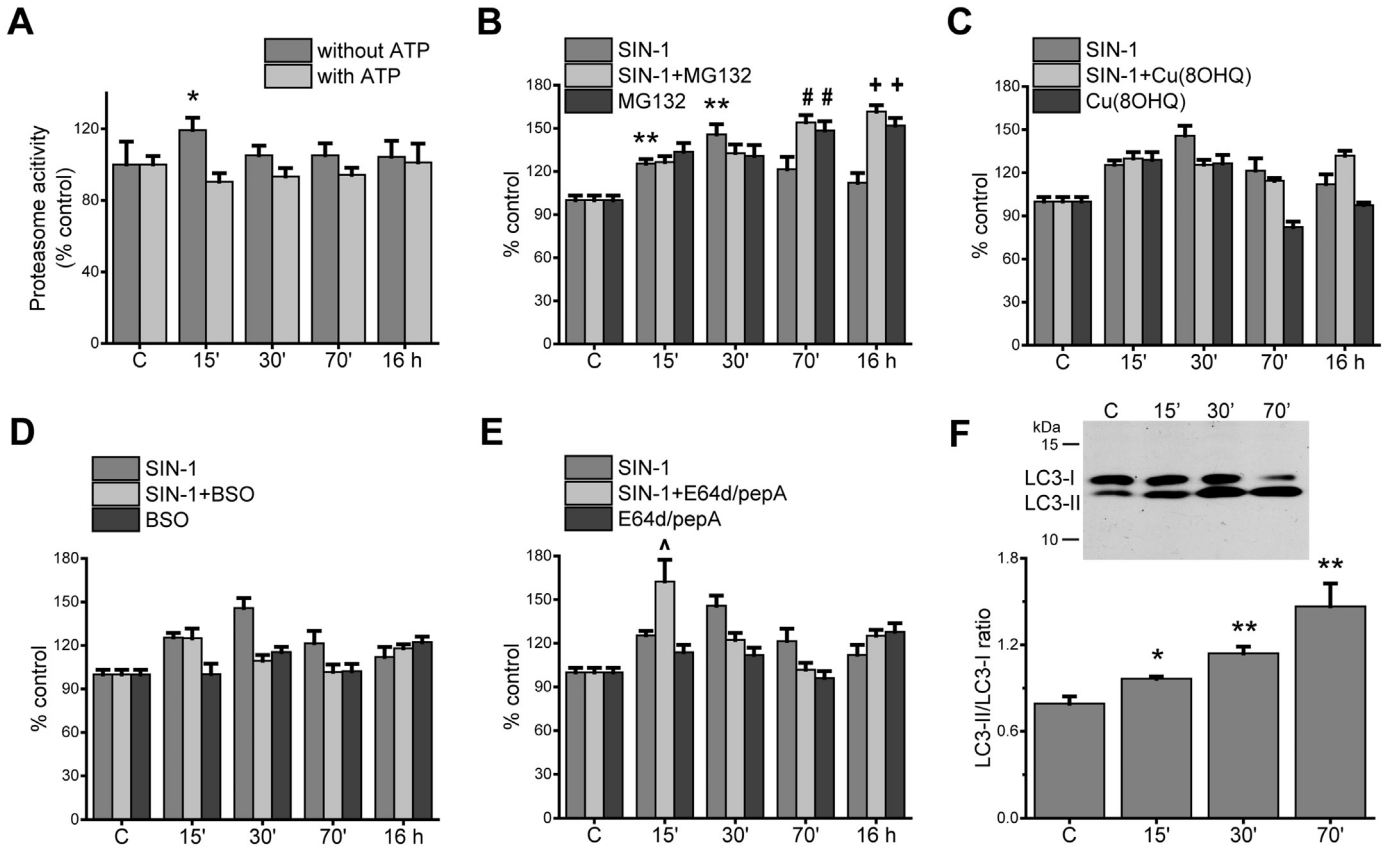

Fig. 2. : Evaluation of detoxification/degradation pathways for carbonylated proteins and lipids in SIN-1 treated cardiomyocytes. (A) Proteasome activity was measured in the absence and presence of ATP (4.2 mmol/L) using the fluorigenic peptide suc-LLVY-AMC as substrate. Data is shown as means ± SE (* $p < 0.05$ vs. control). Assay was performed in 4 independent experiments (3 measurements in each experiment). (B-E) Cells were treated with 10 μM SIN-1 in the absence or presence of inhibitors or with inhibitors alone. Cells were fixed with PFA, labelled with CHH and levels of carbonylation were evaluated by fluorescence microscopy. Images were acquired using a 10x objective (NA 0.25) and quantified by ImageJ. Data is shown as means ± SE (** $p < 0.01$ vs. control, # $p < 0.05$ vs. 70 min SIN-1, + $p < 0.01$ vs. 16 h SIN-1, ^ $p < 0.05$ vs. 15 min SIN-1) of nine images obtained from three independent experiments. Results were normalized to cell numbers obtained by crystal violet staining. The following inhibitors were used: (B) MG132, inhibitor of the proteasomal chymotrypsin-like activity, (C) complex of 8-hydroxyquinoline and $CuSO_4$, inhibitor of the proteasomal chymotrypsin-like activity, (D) buthionine sulfoximine, inhibitor of γ-glutamylcysteine synthetase and (E) E64d and pepstatin A, inhibitors of lysosomal proteases. (F) Western Blot analysis of LC3-I and LC3-II protein abundances. Image is representative of three independent experiments. Ratios of LC3-II to LC3-I were quantified using ImageJ. Data is shown as means ± SE (* $p < 0.05$, ** $p < 0.01$ vs. control).

nylation and inhibition of autophagy/lysosomal degradation pathway, intracellular lipid and oxidized phosphatidylcholine (oxPC) species were monitored in SIN-1 treated cells using fluorescence microscopy. Nile red staining of neutral lipids revealed significant increase in lipid droplets (LDs)-like structures already 15 min upon SIN-1 treatment (Fig. 3A). This effect was persistent for the 30 and 70 min time points and diminished after 16 h. SIN-1 treatment in the presence of E64d/pepstatin A resulted in drastic increase in LDs-like structures with maximal intensities at 30 and 70 min. Similarly, accumulation of oxPC lipids, monitored by natural antibody E06, demonstrated increase in oxPC species at 15 min after SIN-1 treatment followed by enhanced accumulation of oxidized lipids after 30 and 70 min (Fig. 3B). In agreement with the results described above, the level of oxPC returned to the control level 16 h after SIN-1 treatment. Inhibition of autophagy/lysosomal degradation pathway in the presence of SIN-1 resulted in significant accumulation of oxidized lipids at 30 and 70 min in comparison to the cells treated only with SIN-1. Interestingly, the effect was persistent even 16 h after stress induction.

Normally, there is little LD accumulation within the myocardium under normal physiological conditions, suggesting a fine regulation between fatty acid uptake and β-oxidation. However, LDs are found in CM under pathophysiological conditions including many CVDs, obesity, type 2 diabetes and metabolic syndrome [76,77]. Imbalance between fatty acid uptake and β-oxidation or defects in metabolic pathways can result in accumulation of long chain fatty acids and their incorporation in triacylglycerides and phospholipids followed by LD formation. LDs represent dynamic cellular organelles closely correlating with stress response and regulation of metabolic homeostasis [78]. LDs derive from the ER membrane and usually maintain close connection with both ER and mitochondria. Moreover, lipolysis of lipids stored in LDs is mediated via cytoplasmic or lysosomal lipases. Although it is still relatively unclear how LDs are targeted for autophagy/lysosomal degradation, it was demonstrated that autophagy actively participates in LDs dynamics and can consume a whole LD or parts of it [79–81].

Our results confirm a close correlation between LDs dynamics and autophagy/lysosomal degradation pathway. Within the first 15 min upon nitroxidative stress induction, CM respond to metabolic alterations via LDs accumulation. This effect is still visible after 30 min and to a lower extent 70 min after SIN-1 treatment (Fig. 3A). Inhibition of the lysosomal pathway in the presence of SIN-1 clearly increases LD-like structure accumulation with a maximum at 30 min after treatment. Furthermore, similar dynamics were shown for oxPC species (Fig. 3B). Interestingly, signals of oxPC lipids in SIN-1 and inhibitor treated cells closely resemble dot-like structures similar to LDs. Although, co-localization experiments would be required to confirm this finding, accumulation of oxPC lipids might occur on the LD surface monolayer. The presence of oxidized triacylglycerols in the hydrophobic LDs core of dendritic cells in tumor-bearing mice and primary human placental trophoblasts upon hypoxia-induced dyslipidemia was already demonstrated [82]. However, less is known about peroxidation of LD-associated PLs.

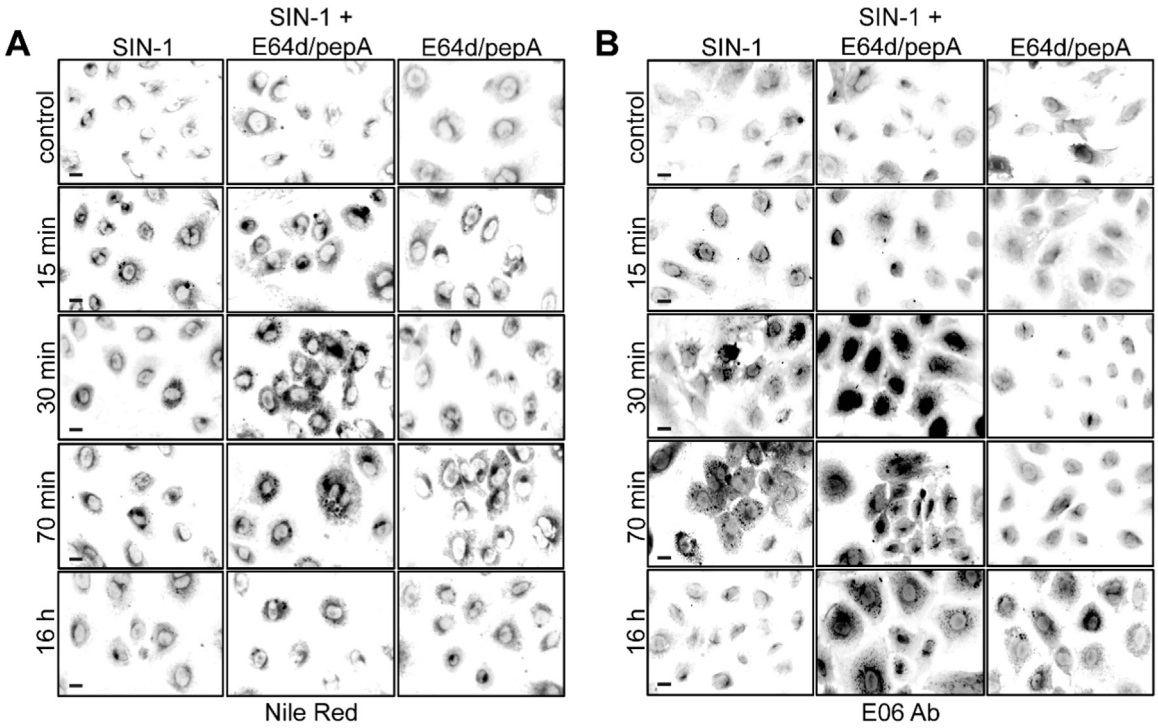

Fig. 3. : Fluorescence microscopy of neutral lipids (A) and oxidized PC (B) in cardiomyocytes treated with SIN-1 in the presence or absence of inhibitors of lysosomal proteases. (A) Cells were stained with Nile Red (1 µg/mL). Nuclei were counterstained with Hoechst 33258. Images are representatives of three independent experiments performed in triplicates. (B) Cells were probed with E06-mAb-TopFluor® (1:100). Nuclei were counterstained with Hoechst 33258. Images are representatives of three independent experiments performed in triplicates. Scale bars 10 µm.

Overall, the results presented above illustrate intensive lipid oxidation at the early time points after stress induction (15 and 30 min) followed by protein carbonylation at the later time points (30 and 70 min). Furthermore, proteasomal degradation plays an important role in the removal of modified proteins at the later time points, whereas the autophagy/lysosomal pathway is responsible for the degradation of carbonylated lipids at the early stages.

3.4. LC-MS based quantification of low molecular weight aldehydes derived from lipid oxidation

Protein carbonylation can occur via several major pathways including direct oxidation of amino acid residues, glycoxidation in the presence of reducing sugars or via Michael addition of electrophilic oxoLPPs to nucleophilic amino acid residues. It is speculated that Michael adducts between proteins and oxoLPPs represent up to 80% of total protein carbonylation [83,84]. This assumption could explain the dynamics of carbonylation events observed here in SIN-1 treated CM. Thus, free radical species formed upon SIN-1 treatment induce lipid peroxidation, resulting in a large pool of electrophilic species carrying aldehyde and/or keto functional groups. These reactive electrophiles in turn can react with nearby proteins inducing their modifications via Michael addition mechanism shifting the carbonylation signal to the protein fraction.

Here we quantified low molecular weight carbonyls produced by lipid peroxidation (oxoLPPs) using carbonyl specific derivatization (CHH) followed by reversed phase LC-MS analysis (Table 1). Overall, 25 different low molecular weight oxoLPPs were detected and their identity was confirmed in tandem mass spectrometry experiments. High resolution and mass accuracy of the orbitrap mass analyzer allowed separation and identification of CHH-derivatized carbonyls with close *m/z* such as heptanal (*m/z* of CHH adduct 372.23) and hydroxy-hexenal (*m/z* 327.19), or decanal (*m/z* 414.28) and hydroxy-nonenal (*m/z* 414.24). Detected oxoLPPs were divided into six structural groups including alkanals, (hydroxy-)alkenals, hydroxy-alkadienals, alkatrienals, oxo-carboxylic acids and dicarbonyls. It was possible to perform relative quantification for 19 out of 25 detected and identified oxoLPPs. Intensities of six remaining signals (hexanal, heptanal, hexenal, hydroxy-hexenal, dodecatrienal and oxo-pentanal) were below the linear dynamic range for all samples used in this study.

Most of the detected oxoLPPs showed a rapid increase in abundance at 15 and 30 min after stress induction. For instance, the concentration of one of the best studied oxoLPPs, hydroxy-nonenal (HNE), increased to 143% of control level already at 15 min, followed by drastic increase to 358% and 309% after 30 and 70 min of SIN-1 treatment, respectively. HNE levels decreased after 16 h to 266% of the control. Similar dynamics were observed for other electrophiles including dicarbonyls such as methylglyoxal/malondialdehyde (MDA) (isomeric species with elemental composition $C_3H_4O_2$ which could not be resolved by the method used here) and oxo-butanal. However, some oxoLPPs showed maximum abundance at 70 min (e.g. nonanal, decanal, undecatrienal) or even 16 h (e.g. octanal, undecanal, dodecanal, nonenal, oxo-nonanoic and oxo-decanoic acids).

The maximum number of species was detected for six and nine carbon long oxoLPPs, which is in good agreement with the most prominent oxidative cleavage sites at the position of double bonds in *n*-3 and *n*-6 polyunsaturated fatty acids. Three of four C6 oxoLPPs were out of linearity range of the method applied and thus were not relatively quantified. However, it was possible to perform relative quantification of all four C9 aldehydes (Fig. S5).

LC-MS based relative quantification revealed a significant increase in the abundance of low molecular weight oxoLPP species at the early time points (15 and 30 min) upon OS induction, confirming the results of microscopy based quantification of carbonylated species in CM. Most of the detected oxoLPPs are strong electrophiles capable of modifying nucleophilic groups in cellular proteins, resulting in an accumulation of oxoLPP-protein adducts. To identify possible targets of oxoLPP-derived modifications, several analytical strategies were used for the analysis of protein extracts from SIN-1 treated CM.

Table 1
Relative quantification of low molecular weight oxoLPP species in SIN-1 treated cardiomyocytes shown as a percentage to untreated samples (control=100%). oxoLPP were derivatized with CHH and quantified using LC-MS. Elemental composition and monoisotopic mass for each oxoLPP are provided as well as *m/z* of the CHH-oxoLPP ion signal used for quantification.

Proposed aldehyde	Elemental composition	Monoisotopic mass	*m/z* after derivatization	RT	15 min/C	30 min/C	70 min/C	16 h/C
					% relative to control ± SE			
Alkanals								
Pentanal	$C_5H_{10}O$	86.07	344.20	6.7	180.8 ± 3.3	192.2 ± 2.9	157.1 ± 7.4	145.8 ± 8.8
Hexanal	$C_6H_{12}O$	100.09	358.21	7.4	NQ	NQ	NQ	NQ
Heptanal	$C_7H_{14}O$	114.10	372.23	7.7	NQ	NQ	NQ	NQ
Octanal	$C_8H_{16}O$	128.12	386.24	8.1	75.1 ± 6.0	96.1 ± 16.7	110.8 ± 16.8	215.7 ± 0.1
Nonanal	$C_9H_{18}O$	142.14	400.26	8.4	111.5 ± 12.8	158.6 ± 23.9	201.5 ± 38.8	197.4 ± 31.9
Decanal	$C_{10}H_{20}O$	156.15	414.28	8.7	94.2 ± 8.9	66.3 ± 21.5	147.3 ± 18.3	121.4 ± 13.8
Undecanal	$C_{11}H_{22}O$	170.17	428.29	8.9	79.0 ± 5.5	47.8 ± 6.1	104.0 ± 7.5	153.5 ± 14.2
Dodecanal	$C_{12}H_{24}O$	184.18	442.31	9.1	74.3 ± 1.3	172.4 ± 18.0	202.4 ± 51.2	206.4 ± 45.7
(Hydroxy-)Alkenals								
Hexenal	$C_6H_{10}O$	98.07	356.20	7.5	NQ	NQ	NQ	NQ
Hydroxy-hexenal	$C_6H_{10}O_2$	114.07	372.19	9.0	NQ	NQ	NQ	NQ
Nonenal	$C_9H_{16}O$	140.12	398.24	8.2	78.8 ± 2.8	130.3 ± 13.7	149.6 ± 14.3	215.0 ± 43.9
Hydroxy-nonenal	$C_9H_{16}O_2$	156.12	414.24	9.6	143.2 ± 21.2	358.2 ± 35.6	308.9 ± 11.1	266.2 ± 48.3
Hydroxy-alkadienals								
Hydroxy-decadienal	$C_{10}H_{16}O_2$	168.12	426.24	7.1	118.11 ± 6.4	144.9 ± 13.7	140.9 ± 3.5	206.9 ± 7.6
Alkatrienals								
Decatrienal	$C_{10}H_{14}O$	150.10	408.23	8.1	94.6 ± 3.7	134.3 ± 2.8	129.0 ± 15.4	178.0 ± 23.1
Undecatrienal	$C_{11}H_{16}O$	164.12	422.24	8.3	72.8 ± 1.4	161.1 ± 16.3	193.5 ± 48.7	191.4 ± 41.7
Dodecatrienal	$C_{12}H_{18}O$	178.14	436.26	8.6	NQ	NQ	NQ	NQ
Oxo-carboxylic acids								
Oxo-hexanoic	$C_6H_{10}O_3$	130.06	388.19	6.1	118.8 ± 12.6	63.6 ± 2.8	45.6 ± 7.0	98.5 ± 6.9
Oxo-octanoic	$C_8H_{14}O_3$	158.09	416.22	6.3	116.0 ± 1.7	133.6 ± 15.2	99.1 ± 0.1	129.0 ± 2.5
Oxo-nonanoic	$C_9H_{16}O_3$	172.11	430.23	6.7	165.6 ± 3.0	195.2 ± 36.3	209.7 ± 51.7	215.1 ± 20.1
Oxo-decanoic	$C_{10}H_{18}O_3$	186.13	444.25	7.5	118.0 ± 5.0	123.4 ± 15.1	159.7 ± 25.8	212.1 ± 14.3
Dicarbonyls								
Glyoxal	$C_2H_2O_2$	58.01	573.25	7.5	74.2 ± 3.4	109.8 ± 8.8	110.3 ± 12.8	166.1 ± 30.0
Malondialdehyde/ Methylglyoxal	$C_3H_4O_2$	72.02	587.26	7.8	81.9 ± 16.7	259.8 ± 29.8	255.8 ± 2.1	190.6 ± 6.3
Oxo-butanal	$C_4H_6O_2$	86.04	601.28	8.1	123.4 ± 7.0	275.2 ± 19.7	197.4 ± 23.0	164.1 ± 1.7
Oxo-pentanal	$C_5H_8O_2$	100.05	615.71	8.9	NQ	NQ	NQ	NQ

3.5. MS strategy for the identification of oxoLPP modified proteins

Proteins can be modified by reactive oxoLPPs via at least two different mechanisms. All oxoLPPs including saturated aldehydes (alkanals) and oxo-carboxylic acids can modify amino groups of Lys- and Arg-residues side chains via Schiff base formation, whereas α,β-unsaturated aldehydes [(hydroxy-)alkenals, hydroxy-alkadienals and alkatrienals] can additionally form Michael adducts with Lys-, Cys- and His-residues [21]. Furthermore, reaction products between protein-bound nucleophiles and dicarbonyls are even more diverse. For instance, glyoxal forms carboxymethyl-derivatives and hemiaminal-adducts with Lys and Arg and dihydroxyimidazolidine with Arg (Fig. 4) [85,86]. To address all modification types, the analysis of oxoLPP modified proteins was performed by two independent bottom-up proteomics strategies (Scheme 1).

Proteins modified via Michael addition retain the oxoLPP carbonyl moiety which can be used for specific derivatization and enrichment prior to LC-MS/MS analysis. Additionally, hemiaminals and Schiff base adducts of dicarbonyls contain the carbonyl function accessible to labeling (Fig. 4). Here we employed derivatization of carbonylated tryptic peptides using aldehyde reactive probe (ARP) followed by biotin-avidin affinity enrichment and RPC-ESI-MS/MS analysis [44] (Scheme 1, right panel). Proteins modified by oxoLPPs via Schiff base formation as well as some intact dicarbonyl modifications, e.g. carboxymethylarginine and dihydroxyimidazolidine, do not contain the carbonyl function and thus cannot be enriched from complex biological samples (Fig. 4). To reduce sample complexity and to access low abundant modified peptides, cell protein extracts were separated by SDS-PAGE, five equal bands were cut out from each lane and subjected to tryptic digestion. Peptides were analysed by RPC-ESI-MS/MS using data-dependent acquisition (DDA) with CID and ETD fragmentation. After initial LC-MS/MS analysis, sample-specific exclusion lists containing *m/z* values and retention times of abundant unmodified peptides were created and used for subsequent DDA analysis (Scheme 1, left panel).

Identification of protein post-translational modifications (PTMs) from bottom-up proteomics experiments is usually achieved via search engine assisted data base search, where mass increments corresponding to the PTMs of interest are included as variable modifications. However, this approach requires a prior knowledge of the modification specific mass increments. Thus, many proteomics experiments, aiming for the identification of oxoLPP-protein adducts, rely only on a few well-known oxoLPP species, such as HNE, hydroxy-hexenal (HHE), glyoxal, methylglyoxal and acrolein, assuming their presence in the sample [44,87–89]. Alternatively, a number of database [90] or spectral library [91–93] search strategies for the identification of peptides with unconsidered PTMs are available, but require higher computational powers.

Here, we combined oxolipidomic and proteomic approaches to characterize sample specific oxoLPP-protein adducts. Thus, a library of 25 sample-specific oxoLPP species was used for data-driven identification of protein adducts in proteomics datasets. For that, a list of mass increments corresponding to oxoLPP Michael adducts/intact dicarbonyls (molecular weight of the aldehyde) or Schiff bases (molecular weight of the aldehyde minus 18 units corresponding to the loss of water) was constructed and used to define variable modifications for

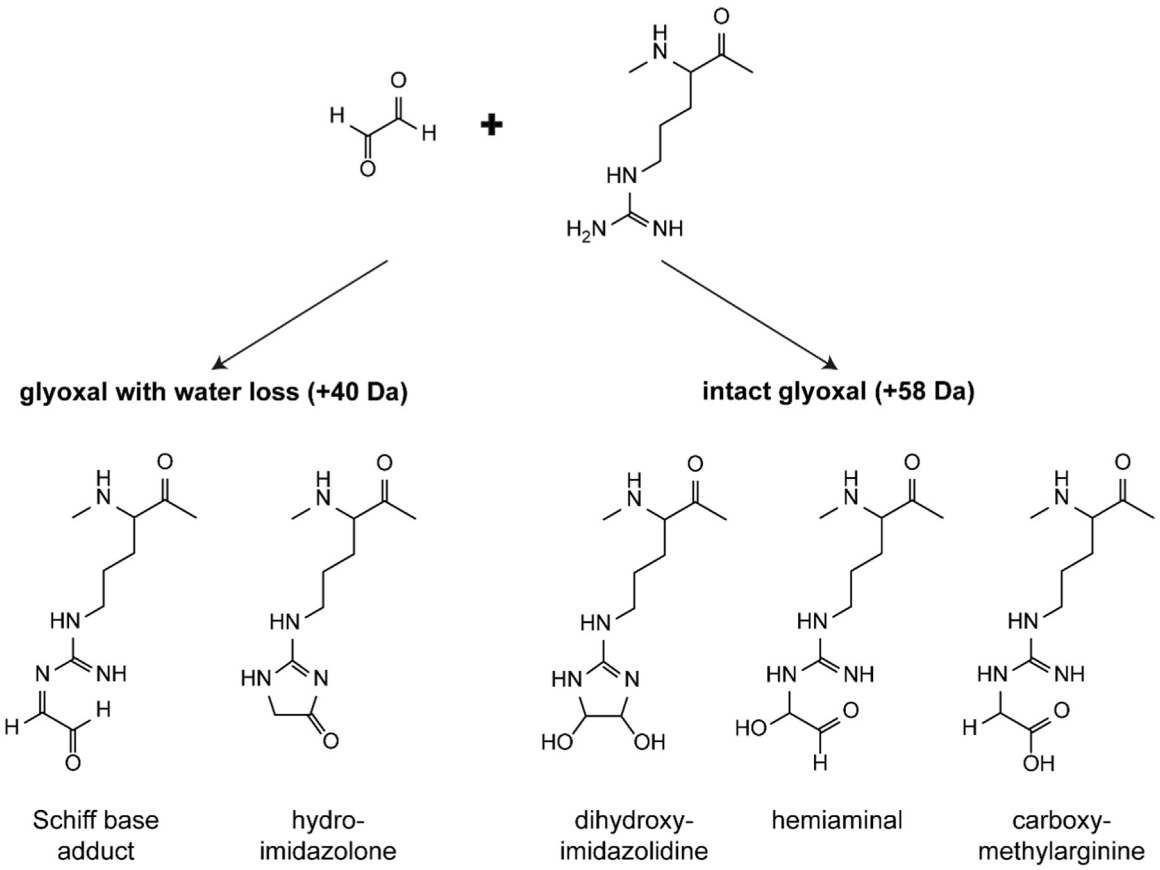

Fig. 4. : Illustration of possible adducts between Arg amino acid residue and glyoxal. Reaction of arginine with the intact glyoxal can result in carboxymethylarginine, glyoxal-derived dihydroxyimidazolidine and/or glyoxal-hemiaminal. When the reaction is followed by a water loss, the Schiff base adduct and/or glyoxal-derived hydroimidazolone are formed.

search engine assisted database search (Table S1).

To confirm identifications by database searches tandem spectra were manually assigned. For instance, the ETD-spectrum of the precursor ion at *m/z* 513.76 (z=4, RT=19.14) was identified as vimentin peptide ^{144}SRLGDLYEEEMRELR^{158} (Fig. 5A). The complete $c_{2\text{-}14}$ and $z_{4\text{-}14}$ ion-series were assigned indicating oxo-octanoic acid Schiff base modification on Arg155 (mass increment of 140.1 units). Additionally, Met sulfoxide in position 154 was detected (mass increment of 16.0 units). The combined neutral loss of oxo-octanoic acid and water was observed in form of the charge reduced ion $[M+3H^{+}\text{-}C_8H_{12}O_2\text{-}H_2O]^{2+}$ at *m/z* 948.7.

The ETD spectrum of the precursor ion at *m/z* 678.98 (z=3, RT=15.94) allowed its assignment to the peptide ^{69}YPIEHGIVTNWDDMEK^{84} of cytoplasmic actin 1 modified by intact methylglyoxal/MDA (Fig. 5B). Almost complete c-ion-series (c_3-c_5, c_7 and c_9-c_{15}) and 9 out of 15 possible *z* ions (z_2-z_5, z_7 and z_{11}-z_{14}) were assigned and allowed confirmation of the presence of methylglyoxal/MDA characteristic mass increment (+72.0 units) and sulfoxide (+16.0 units) on His73 and Met81, respectively. The neutral loss of methylglyoxal/MDA and water from the precursor ion further confirmed the identified modification.

The CID-spectrum of the precursor ion with *m/z* 1013.07 (z=2, RT=22.14 min) was assigned to the tryptic peptide ^{106}AKTKPVAFAVRTNVR^{120} of the voltage-dependent L-type calcium channel subunit beta-2 (Fig. 5C) modified by ARP-derivatized methylglyoxal/MDA Schiff base. Almost complete *b*-ion series (b_4, b_6-b_{11} and b_{14}) could be assigned of which all signals carried the characteristic mass increment of 367.1 units (ARP derivatized methylglyoxal/MDA Schiff base). Six out of 14 possible *y*-ions (y_3, y_5-y_6, y_8, y_{11}, and y_{14}) were detected of which the y_{14} ion with the oxoLPP specific increment allowed assignment of the modification to Lys107.

The peptide with *m/z* 598.10 (z=4, RT=14.96 min) was identified as peptide ^{3289}LAVFSQPIINKVKPQLLK^{3306} of the ryanodine receptor type 2 (Fig. 5D). Seven out of 17 CID derived *b*-ions were detected (b_3, b_5, b_8-b_9, b_{11}, b_{15}, and b_{17}), with the last three carrying the mass increment specific for ARP-derivatized glyoxal Schiff base (353.1 units). Nine out of 17 possible *y*-ions were assigned (y_8-y_{17}), all of which had a mass increment of 353.1 units. Thus, modification was localized to Lys3299. Accuracy of the assignment was further confirmed by the presence of an ARP specific fragment ion (*m/z* 227.09) and neutral losses (ARP neutral loss from doubly charged precursor and y_9-ion).

Using data-driven proteomics identification we were able to identify a total of 99 unique proteins modified by oxoLPPs via Schiff base formation and by intact dicarbonyls (Fig. 6A). 39 proteins were present in control and SIN-1 treated samples, whereas 19 and 41 proteins were unique for control and SIN-1 treated cells, respectively. It is important to note, that the analytical approach used here allowed only identification but not quantification of modified peptides. Thus, no conclusions on the absolute or relative quantities of modified proteins can be drawn from these results.

23 proteins modified by dicarbonyls via Schiff base were represented by 25 tryptic peptides containing 30 modification sites, while 67 proteins showed modifications by intact dicarbonyls represented by 86 peptides containing 135 modification sites. With 45 modification sites oxo-butanal was the most abundant modification as intact dicarbonyl followed by oxo-pentanal [40] and methylglyoxal/MDA [31]. Lys (63 modification sites, 44%) and Arg (45, 31%) were more often modified with dicarbonyls than Cys (15, 10%) and His (20, 14%) (Fig. 6B).

All other oxoLPPs (alkanals, (hydroxy-)alkenals, hydroxy-alkadienals, alkatrienals, carboxylic acids) were identified as Schiff base modifications on 29 proteins with 35 peptides containing 42 modifica-

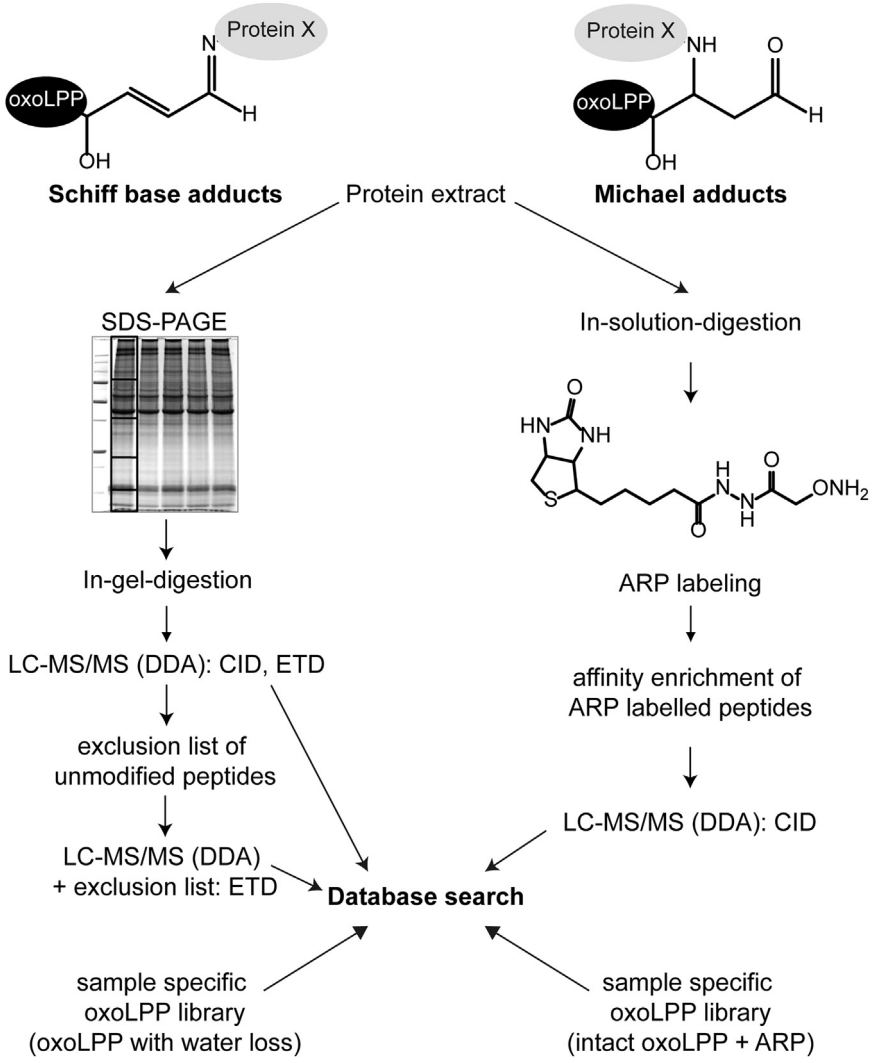

Scheme 1. Schematic representation of bottom-up proteomics strategies used for identification of oxoLPP-protein adducts.

tion sites (Tables S2 and S3). The most abundant Schiff base adduct was methylglyoxal/MDA detected for 11 modification sites, followed by glyoxal [10], oxo-butanal [9] and oxo-nonanoic acid [6] (Fig. 6C). In general, short carbon chain oxoLPPs, especially dicarbonyls, showed significantly higher number of modification sites. It has to be noted that the reactions of oxo-nonanoic acid via Schiff base formation and oxo-nonenal via Michael addition result in exactly the same mass increment. At this point we cannot distinguish between those two different oxoLPPs, which is also the case for the other oxo-carboxylic acids and oxo-alkenals (e.g. oxo-hexanoic acid/oxo-hexenal). With 42 modification sites Lys was slightly more susceptible to Schiff base formation than Arg (36 modification sites).

For the identification of carbonylated proteins oxoLPP Michael adducts on Cys, His and Lys, hemiaminal formation of dicarbonyls on Lys, Cys, His and Arg, Schiff base adducts of dicarbonyls on Lys and Arg and direct oxidation (often referred as metal-catalysed oxidation [MCO]) on Pro, Lys, Thr and Arg were considered. ARP labeling and affinity enrichment of modified peptides followed by RPC-MS/MS detection allowed identification of 74 unique carbonylated proteins represented by 107 unique modified peptides with 135 modification sites (Tables S4 and S5). 21 proteins were common for both control and SIN-1 treated cells (Fig. 7A). Only 8 unique proteins were identified in the control whereas 45 carbonylated proteins were present only after SIN-1 treatment.

28 modification sites in 18 proteins were assigned to carbonylation via direct oxidation, with Lys being the most susceptible (50%) modification site followed by Pro (25%), Arg (18%) and Thr (7%) (Fig. 7B). Five identified modification sites (all Lys) were assigned to elastin and are known to occur via enzymatic reaction with lysyl oxidase (LOX) [94]. Removing them from the calculation provides close susceptibility for Lys (39%) and Pro (30%), followed by Arg (22%) and Thr (9%). Lys and Pro were already identified as the most susceptible amino acids for MCO by different research groups [95,96].

26 proteins (41 modification sites) were identified as oxoLPP Michael adducts, 25 proteins (35 modification sites) corresponded to dicarbonyl hemiaminals and 29 (31 modification sites) to dicarbonyl Schiff bases. Similar to the Schiff base modifications, oxoLPPs assigned to the highest number of modification sites corresponded to reactive carbonyls with short carbon chains. More precisely, dicarbonyl hemiaminals and Schiff bases were the most often identified modifications (Fig. 7C). Thus, glyoxal, methylglyoxal/MDA, oxo-butanal and oxo-pentanal resulted in 66 out of 135 modification sites in total. The second type of the most reactive oxoLPPs corresponded to α,β-unsaturated aldehydes such as hexenal and nonenal as well as their hydroxylated forms, with HNE being the most abundant one (9 modification sites). The most abundant modified amino acid was Lys (47%) followed by Arg (20%), Cys (19%) and His (14%). Modification sites of the four dicarbonyls reacting to proteins via Schiff base were not considered for this calculation.

High reactivity of dicarbonyls towards nucleophilic groups can be

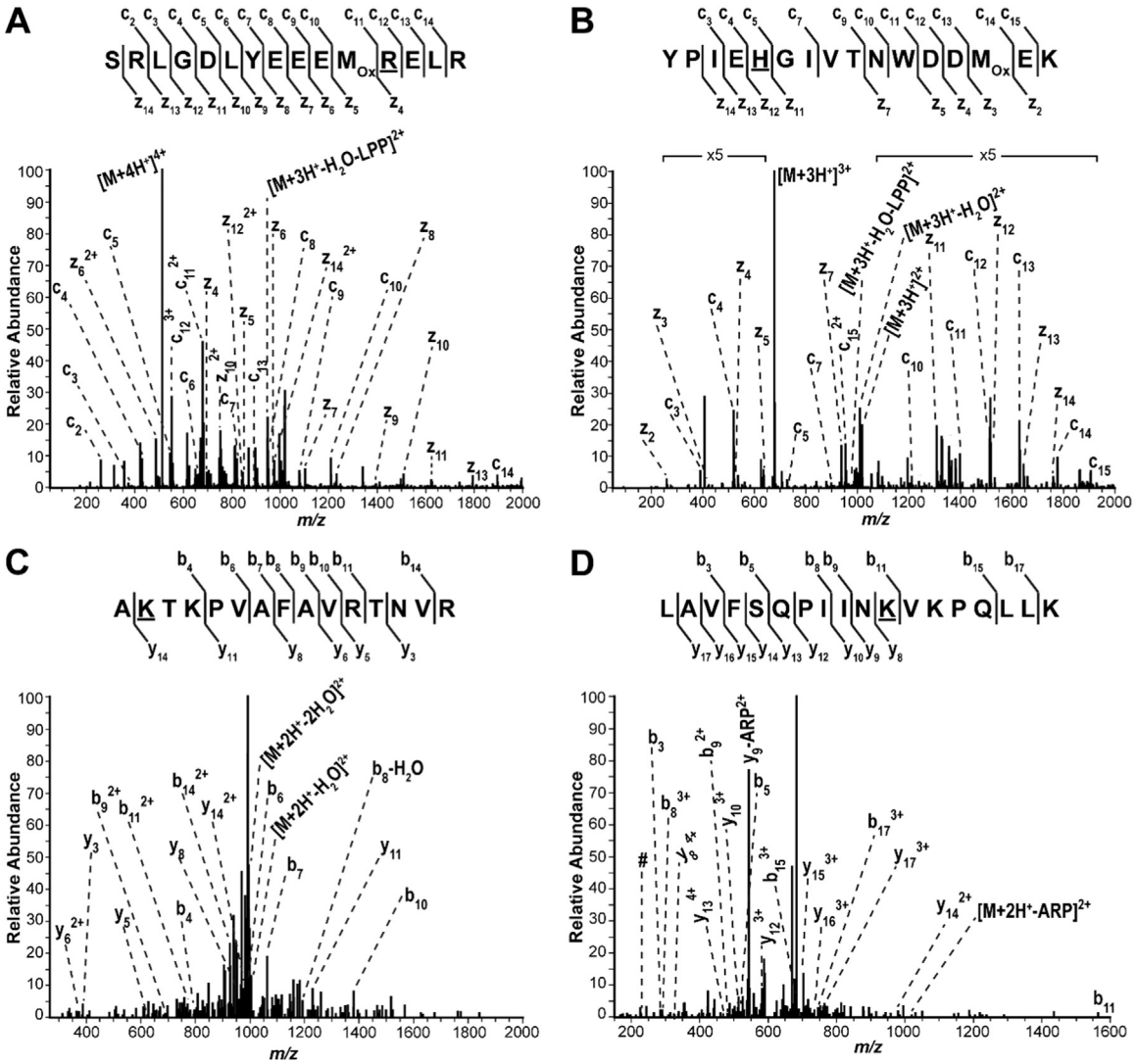

Fig. 5. : LTQ-Orbitrap ETD- and CID mass spectra of oxoLPP modified peptides. (A) Arg155 of vimentin was modified with oxo-octanoic acid via Schiff base formation. (B) His73 of cytoplasmic actin 1 was modified with intact methylglyoxal/MDA. (C) Lys107 of voltage-dependent L-type calcium channel subunit beta-2 was modified with ARP-derivatized methylglyoxal/MDA via Schiff base formation. (D) Lys3299 of ryanodine receptor type 2 was modified with ARP-derivatized glyoxal via Schiff base formation. # refers to the ARP-specific fragment *m/z* 227.

explained using the Hard and Soft, Acids and Bases (HSAB) theory of Pearson. Presence of the second carbonyl function (assuming it is in α position) results in a higher electrophilicity of the first carbonyl group. Indeed, glyoxal, shown here as the most reactive oxoLPP (15 modification sites), was recently classified as aldehyde with the highest calculated electrophilicity and softness [97], followed by HNE, MDA and HHE [98], which closely resembled the reactivity detected in our study (nine, ten and five modification sites for HNE, methylglyoxal/MDA and HHE respectively). One more reason for the high reactivity of short chain dicarbonyls could be the relatively high hydrophilicity. It was demonstrated that peptides as relatively hydrophilic substrates preferentially react with shorter carbon chain aldehydes whereas aminophospholipids, as more hydrophobic compounds, are modified with longer chain carbonylated analogues [99].

Relatively soft aldehydes such as dicarbonyls should preferentially react with Cys (soft nucleophile), however, Lys, His and Arg were shown to be modified as well. It is important to take the natural abundances of the amino acids into account considering for example the difference between Lys (6.19%) and Cys (2.01%) within the proteins of this dataset. Normalization of the results to the amino acid abundance across the 169 identified proteins confirmed Cys as the most susceptible modification site (35%), followed by Lys (29%), His (23%) and Arg (13%). Normalization of the results to the amino acid abundance in the rat proteome (Lys – 5.65%, Cys – 2.15%) leads to closer susceptibility of Cys (33%) and Lys (31.7%).

3.6. Functional assignment of oxoLPP-modified proteins

Overall 167 unique proteins were identified to be modified by MCO, intact dicarbonyls (including hemiaminals), (hydroxy-)alkenals via Michael addition or all aldehydes via Schiff base formation in control and SIN-1 treated CM. The majority of the proteins were identified based on one, two and three modified residues (78, 56 and 17 unique identifications respectively). Seven proteins (cytoplasmic dynein 2 heavy chain 1, regulator of G-protein signaling 7, neurofibromin, fatty acid synthase, putative RNA exonuclease NEF-sp, dimethylaniline monooxygenase, synergin gamma) were detected with four modified positions each. Four proteins (YLP motif-containing protein 1, HORMA domain-containing protein 1, elastin, vimentin) had five modification sites. Among the most modified proteins were slit homolog 3 protein, E3 ubiquitin-protein ligase UBR4, serine/threonine-protein kinase WNK1, actin isoforms and fibronectin with six, seven, eight, ten and twelve modified residues, respectively. Interestingly, all five modified residues in elastin and three out of

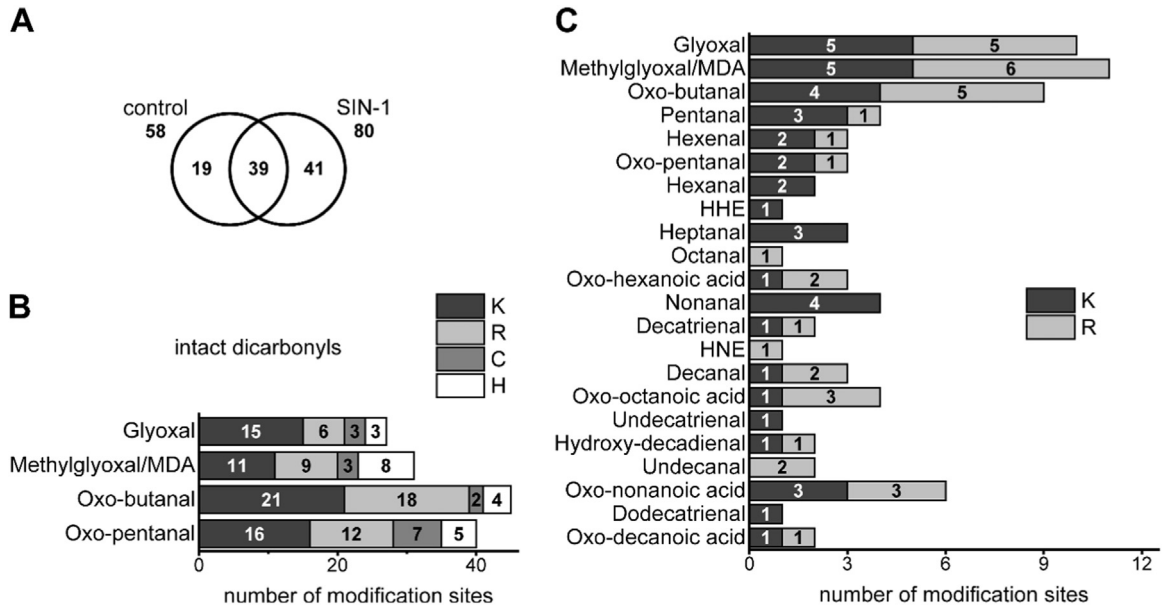

Fig. 6. : Summary of results obtained by LC-MS/MS analysis of proteins modified with oxoLPPs via Schiff base formation or intact dicarbonyls in SIN-1 treated cardiomyocytes. (A) Venn diagram representing numbers of unique and common Schiff base and intact dicarbonyl modified proteins in control and SIN-1 treated cells. (B) Diagram representing the numbers of amino acid residues modified by the corresponding intact dicarbonyl. (C) Diagram showing the numbers of amino acid residues modified by the corresponding oxoLPP via Schiff base formation. MDA - malondialdehyde, HHE - hydroxy-hexenal, HNE - hydroxy-nonenal.

twelve in fibronectin were identified as ARP-derivatized aminoadipic semialdehydes in all experimental conditions. Enzymatic oxidation of lysine residues in extracellular matrix (ECM) proteins by lysyl oxidase (LOX) is a well-known modification [94]. Among the five carbonylated lysine residues from elastin, three are already reported in UniProtKB (Lys 290, 363 and 680), whereas carbonylation on Lys 231 and 279 was shown here additionally. These results underline the specificity of the ARP-derivatization and enrichment method applied here.

To evaluate functional enrichment and possible interactions of modified proteins STRING network analysis was performed (version 10.0). Reconstructed network showed significant protein-protein interactions enrichment (p-value of $4{,}45e^{-6}$; number of nodes 167, number of edges 106, average node degree 1.27). Furthermore, data showed significant enrichment ($p \leq 0.05$) in 305 and 79 GO-terms for biological processes and molecular functions, respectively. Proteins also showed significant enrichment in four KEGG pathways including calcium signaling pathway (p=0.0014), circadian entrainment (p=0.033), hypertrophic cardiomyopathy (0.033) and dilated cardiomyopathy.

Additionally, all 167 modified proteins were manually annotated based on their gene ontology terms (biological process and molecular function) provided by UniProtKB and classified into 15 categories including proteins involved in cytoskeleton and its regulation [29],

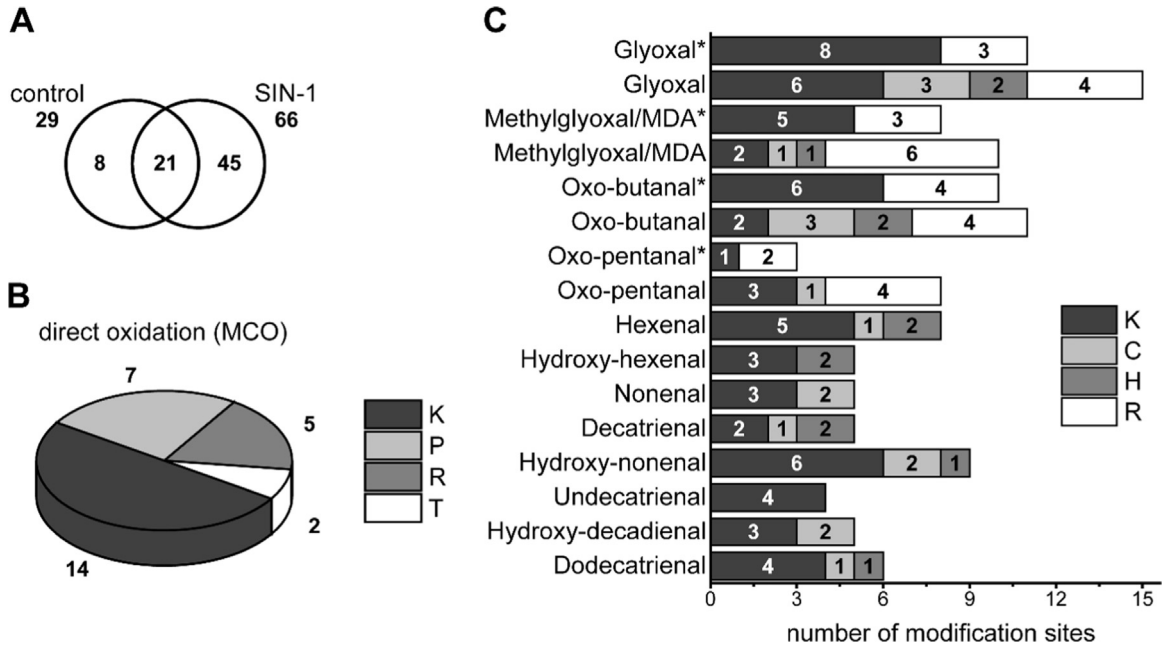

Fig. 7. : Summary of results obtained by LC-MS/MS analysis of proteins carbonylated by oxoLPPs or metal-catalysed oxidation (MCO). (A) Venn diagram representing numbers of unique and common carbonylated proteins in control and SIN-1 treated cells. (B) Diagram representing the numbers of amino acid residues oxidized via MCO. (C) Diagram showing the numbers of amino acid residues modified by the corresponding (hydroxy-)alkenals via Michael addition and dicarbonyls via Schiff base- (*) or hemiaminal-formation. MDA – malondialdehyde.

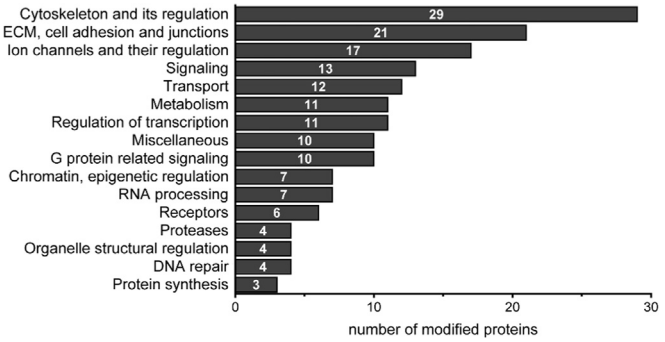

Fig. 8. : Functional assignment of oxoLPP modified proteins in control and SIN-1 treated cardiomyocytes.

ECM, cell adhesion and junctions [21], ion channels and their regulation [17], signaling [13], transport [12], metabolism [11], regulation of transcription [11], G proteins related signaling [10], RNA processing [7], chromatin, epigenetic regulation [7], receptors [6], organelle structure and regulation [4], proteases [4], DNA repair [4], protein synthesis [3], and miscellaneous (10 proteins) (Fig. 8 and Table S6). Modified cytoskeletal proteins included members of microfilaments (actin), intermediate filaments (vimentin, lamin) and microtubules (centrosomal proteins and dynein) as well as several critical regulatory factors, for instance myosin-binding protein C (MyBP-C), important for sarcomeric structure stability and regulation of contraction. MyBP-C carbonylation was previously demonstrated in cardiac tissue from doxorubicin-treated rats and associated with impaired interaction between MyBP-C and F-actin [100]. Besides cytoskeletal proteins, ECM and cell adhesion proteins were among the most abundant modification targets. In addition to the above mentioned enzymatically modified elastin, fibronectin and collagen were modified by reactive oxoLPPs. Interestingly quantification of protein abundances in the human proteome of the U2OS cell line described proteins involved in cell adhesion and calcium signaling to be less abundant [101], which confirms the selectivity of carbonylation and oxoLPP modifications. Cytoskeletal and ECM/cell adhesion proteins were already shown to be preferentially modified by oxoLPPs in fatty-acid treated hepatocytes [53] and in plasma samples from obese/T2DM patients [44]. Ageing associated protein carbonylation showed similar functional groups including cytoskeleton, membrane transport, signaling, metabolism and receptor proteins [102]. Metabolic enzymes such as fatty acid synthase, alcohol dehydrogenase 4, isocitrate dehydrogenase (NAD+) subunit beta, trifunctional enzyme subunit alpha and cytochrome c oxidase subunit 6C-2, identified here as oxoLPPs targets, were reported to be carbonylated previously [102–106]. Carbonylation and HNE-adduction of these enzymes were shown to impair their function [107,108]. With isocitrate dehydrogenase taking part in the TCA-cycle, the trifunctional enzyme in the fatty acid β-oxidation and the cytochrome c oxidase as complex IV in the electron transport chain, these proteins are important for the energy production.

Among modification targets identified here histone H2B type 1 and histone acetyltransferase KAT6A were shown to form adducts with reactive oxoLPPs [53]. Thus, several modification sites of histones with 4-ONE were already reported before in RKO cells treated with 4-ONE. However, only modification of histones H3 and H4, but not H2B, resulted in inhibition of nucleosome assembly [109].

We also identified carbonylation of the serine/threonine-protein kinase mTOR, which was shown before [110]. It is known that mTOR is inhibited by redox modifications, which induces autophagy. As described above autophagy is increased in our cell model. This result suggests that carbonylation of mTOR might lead to its inhibition followed by autophagy stimulation.

Interestingly, 14 proteins assigned to ion transport function (ion channels and their regulation) were found to be modified. Among them six channels are important mediators of calcium signaling including ryanodine receptors 1 and 2, subunits of L-, R- and T-types voltage-dependent calcium channels (VDCC) and inositol 1,4,5-trisphosphate receptor type 3. Calcium signaling is a critical regulator of cardiac function and oxoLPP-derived modifications of key molecular players might significantly compromise CM excitation-contraction-coupling.

3.7. *Effect of protein modifications on Ca^{2+} signaling pathway*

To investigate possible influence of oxoLPP-derived modifications of calcium channels on their activity we measured Ca^{2+} mobilization in non-treated and SIN-1 treated (70 min) cells using channel specific agonists.

When ATP was used to stimulate calcium influx via L-type voltage-dependent calcium channels (VDCC) significant decrease of influx was observed in SIN-1 treated CM in comparison to control (Fig. 9A). On the other hand, SIN-1 treated cells demonstrated elevated Ca^{2+} mobilization in the presence of palmitoyl-oleoyl-glycerophosphate (POPA), which is known to stimulate inositol trisphosphate receptors (Fig. 9B). Surprisingly, SIN-1 treatment did not induce any changes in Ca^{2+} cytoplasmic release upon stimulation of ryanodine receptor 2 with 4-chloro-3-methylphenol (Fig. 9C).

Redox regulation of Ca^{2+} channels activity via oxidative PTMs was reported previously [111,112]. Thus, 21 out of 89 Cys residues of ryanodine receptor (RyR) are present in a reduced form and modifications of these residues via S-nitrosylation were shown to alter channel activity [111,113,114]. During aging, oxidation but not S-nitrosylation or S-glutathionylation of RyR resulted in channel hyperactivity [115]. S-glutathionylation of the voltage-dependent L-type calcium channel resulted in an increased channel open probability [116]. Carbonylation and oxoLPP adducts of Ca^{2+} channels haven't been investigated

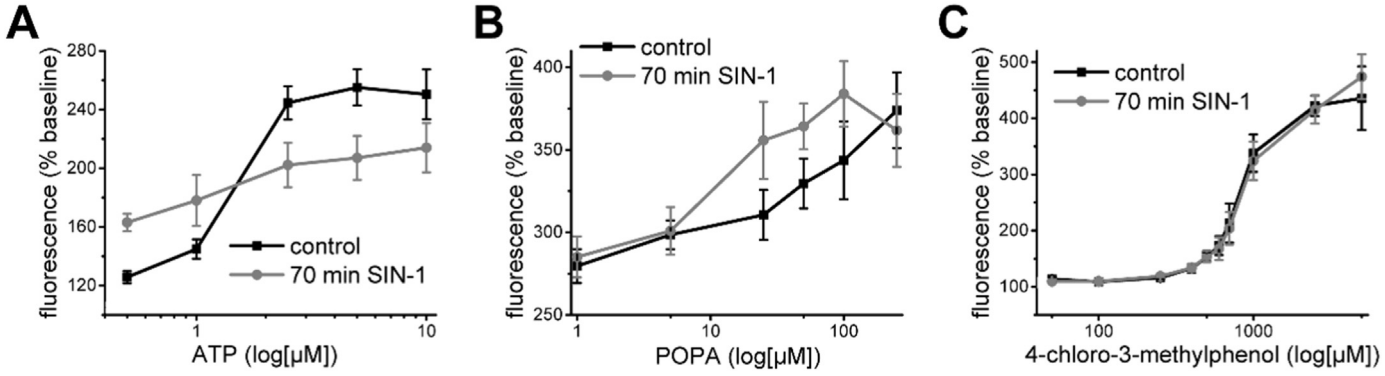

Fig. 9. : Concentration-response curves in SIN-1 treated (70 min) and untreated (control) cardiomyocytes for $[Ca^{2+}]_i$ increase upon stimulation with (A) ATP (agonist of L-type voltage dependent Ca^{2+} channels), (B) palmitoyl-oleoyl-phosphatidic acid (POPA; agonist of inositol 1,4,5-trisphosphate receptors) and (C) 4-chloro-3-methylphenol (agonist of ryanodine receptor 2). Data is shown as means ± SE. Results are representatives of three independent experiments performed in triplicates.

intensively. However, Cai et al. [117] demonstrated a biphasic elevation of intracellular Ca^{2+} in MDA-incubated (30 min) hippocampal neurons with an early phase assigned to Ca^{2+} release from SR via IP_3R and a late phase from Ca^{2+} influx through L-type VDCC. Methylglyoxal-treated (24 h) sensory neurons upon KCl mediated plasma membrane depolarization showed a dual effect on Ca^{2+} influx with an increase of intracellular Ca^{2+} at low methylglyoxal concentrations (up to 150 μM) and a decrease at higher concentrations (250–750 μM) [118]. Albano et al. demonstrated a correlation between elevation of intracellular Ca^{2+} and lipid peroxidation in isolated rat hepatocytes stimulated with $FeCl_3$ [119]. Treatment of hippocampal neurons with HNE (2 h) resulted in an increase of Ca^{2+} influx via VDCCs. However, no HNE-VDCCs adducts were detected and the observed functional effect was attributed to tyrosine phosphorylation [120]. In the diabetic heart methylglyoxal and glyoxal adducts with RyR2 were identified and associated with heterogeneity of channel activity [121]. However, in complex diseases and even cellular models of oxidative stress changes in channel activity cannot be attributed to a single type of PTM. Complete PTM profiling or site-directed mutagenesis studies are required to demonstrate the significance of a modification or a certain amino acid residue for protein activity.

4. Conclusions

Combination of fluorescence microscopy and LC-MS based protocols for detection of carbonylated lipids and proteins allowed monitoring of the time course of biomolecule oxidation and degradation in a dynamic model of nitroxidative stress. Differences in kinetics of lipid and protein carbonylation were demonstrated. A significant role of the autophagy/lysosomal pathway was shown for the degradation of oxidized lipids, whereas the proteasome was mainly responsible for the removal of carbonylated proteins. Lipids are proposed as primary carbonylation targets capable of transferring the carbonyl signal to the protein fraction at later time points. Carbonylated LPP and proteins were identified using a combination of several LC-MS/MS strategies. Molecular identity of sample-specific oxoLPPs allowed performance of data-driven identification of their protein targets, among which several functional groups showed significant enrichment. Alteration in activity of oxoLPP-modified calcium channels was demonstrated.

Acknowledgment

We thank Prof. Ralf Hoffmann (Institute of Bioanalytical Chemistry, University of Leipzig) for providing access to his laboratory and mass spectrometers. The authors are thankful to Dr. Jan Stichel and Prof. Annette Beck-Sickinger (Institute of Biochemistry, University of Leipzig) for providing access to the FlexStation 3 multi-mode microplate reader. Financial support from Deutsche Forschungsgemeinschaft, Germany (DFG; FE-1236/3-1 to M.F.; Gr-1240/16-2 to T.G.), European Regional Development Fund (ERDF, European Union and Free State Saxony; 100146238 and 100121468 to M.F) and COST Action CM1001 are gratefully acknowledged. We acknowledge support from the German Research Foundation (DFG) and Universität Leipzig within the program of Open Access Publishing.

Appendix A. Supplementary material

Supplementary data associated with this article can be found in the online version at doi:10.1016/j.redox.2016.12.028.

References

[1] J.M. Zimmet, J.M. Hare, Nitroso-redox interactions in the cardiovascular system, Circulation 114 (2006) 1531–1544.
[2] V. Cecarini, J. Gee, E. Fioretti, M. Amici, M. Angeletti, A.M. Eleuteri, J.N. Keller, Protein oxidation and cellular homeostasis: emphasis on metabolism, Biochim. Et. Biophys. Acta 1773 (2007) 93–104.
[3] N.S. Dhalla, R.M. Temsah, T. Netticadan, Role of oxidative stress in cardiovascular diseases, J. Hypertens. 18 (2000) 655–673.
[4] R. Rastaldo, P. Pagliaro, S. Cappello, C. Penna, D. Mancardi, N. Westerhof, G. Losano, Nitric oxide and cardiac function, Life Sci. 81 (2007) 779–793.
[5] M.J. Kohr, S.R. Roof, J.L. Zweier, M.T. Ziolo, Modulation of myocardial contraction by peroxynitrite, Front. Physiol. 3 (2012) 468.
[6] C. Szabo, H. Ischiropoulos, R. Radi, Peroxynitrite: biochemistry, pathophysiology and development of therapeutics, Nat. Rev. Drug Discov. 6 (2007) 662–680.
[7] R.M. Uppu, B.D. Nossaman, A.J. Greco, A. Fokin, S.N. Murthy, V.A. Fonseca, P.J. Kadowitz, Cardiovascular effects of peroxynitrite, Clin. Exp. Pharmacol. Physiol. 34 (2007) 933–937.
[8] P.Y. Cheung, W. Wang, R. Schulz, Glutathione protects against myocardial ischemia-reperfusion injury by detoxifying peroxynitrite, J. Mol. Cell. Cardiol. 32 (2000) 1669–1678.
[9] P. Wang, J.L. Zweier, Measurement of nitric oxide and peroxynitrite generation in the postischemic heart. Evidence for peroxynitrite-mediated reperfusion injury, J. Biol. Chem. 271 (1996) 29223–29230.
[10] P. Ferdinandy, H. Danial, I. Ambrus, R.A. Rothery, R. Schulz, Peroxynitrite is a major contributor to cytokine-induced myocardial contractile failure, Circ. Res. 87 (2000) 241–247.
[11] P. Zhang, X. Xu, X. Hu, E.D. van Deel, G. Zhu, Y. Chen, Inducible nitric oxide synthase deficiency protects the heart from systolic overload-induced ventricular hypertrophy and congestive heart failure, Circ. Res. 100 (2007) 1089–1098.
[12] J.S. Luoma, P. Stralin, S.L. Marklund, T.P. Hiltunen, T. Sarkioja, S. Yla-Herttuala, Expression of extracellular SOD and iNOS in macrophages and smooth muscle cells in human and rabbit atherosclerotic lesions: colocalization with epitopes characteristic of oxidized LDL and peroxynitrite-modified proteins, Arterioscler. Thromb. Vasc. Biol. 18 (1998) 157–167.
[13] W.L. Suarez-Pinzon, J.G. Mabley, K. Strynadka, R.F. Power, C. Szabo, A. Rabinovitch, An inhibitor of inducible nitric oxide synthase and scavenger of peroxynitrite prevents diabetes development in NOD mice, J. Autoimmun. 16 (2001) 449–455.
[14] P. Pacher, L. Liaudet, P. Bai, J.G. Mabley, P.M. Kaminski, L. Virag, A. Deb, E. Szabo, Z. Ungvari, M.S. Wolin, J.T. Groves, C. Szabo, Potent metalloporphyrin peroxynitrite decomposition catalyst protects against the development of doxorubicin-induced cardiac dysfunction, Circulation 107 (2003) 896–904.
[15] I.M. Bonilla, A. Sridhar, Y. Nishijima, S. Gyorke, A.J. Cardounel, C.A. Carnes, Differential effects of the peroxynitrite donor, SIN-1, on atrial and ventricular myocyte electrophysiology, J. Cardiovasc. Pharmacol. 61 (2013) 401–407.
[16] C. Szabo, Multiple pathways of peroxynitrite cytotoxicity, Toxicol. Lett. 140–141 (2003) 105–112.
[17] H. Rubbo, A. Trostchansky, V.B. O'Donnell, Peroxynitrite-mediated lipid oxidation and nitration: mechanisms and consequences, Arch. Biochem. Biophys. 484 (2009) 167–172.
[18] S. Dalleau, M. Baradat, F. Gueraud, L. Huc, Cell death and diseases related to oxidative stress: 4-hydroxynonenal (HNE) in the balance, Cell death Differ. 20 (2013) 1615–1630.
[19] I. Dalle-Donne, D. Giustarini, R. Colombo, R. Rossi, A. Milzani, Protein carbonylation in human diseases, Trends Mol. Med. 9 (2003) 169–176.
[20] A. Ayala, M.F. Munoz, S. Arguelles, Lipid peroxidation: production, metabolism, and signaling mechanisms of malondialdehyde and 4-hydroxy-2-nonenal, Oxid. Med. Cell. Longev. 2014 (2014) 360438.
[21] R.M. Domingues, P. Domingues, T. Melo, D. Perez-Sala, A. Reis, C.M. Spickett, Lipoxidation adducts with peptides and proteins: deleterious modifications or signaling mechanisms?, J. Proteom. 92 (2013) 110–131.
[22] G. Aldini, M.R. Domingues, C.M. Spickett, P. Domingues, A. Altomare, F.J. Sanchez-Gomez, C.L. Oeste, D. Perez-Sala, Protein lipoxidation: detection strategies and challenges, Redox Biol. 5 (2015) 253–266.
[23] A. Negre-Salvayre, C. Coatrieux, C. Ingueneau, R. Salvayre, Advanced lipid peroxidation end products in oxidative damage to proteins. Potential role in diseases and therapeutic prospects for the inhibitors, Br. J. Pharmacol. 153 (2008) 6–20.
[24] R. Pamplona, Advanced lipoxidation end-products, Chem.-Biol. Interact. 192 (2011) 14–20.
[25] T. Nystrom, Role of oxidative carbonylation in protein quality control and senescence, EMBO J. 24 (2005) 1311–1317.
[26] D. Conklin, R. Prough, A. Bhatanagar, Aldehyde metabolism in the cardiovascular system, Mol. Biosyst. 3 (2007) 136–150.
[27] D.J. Conklin, Y. Guo, G. Jagatheesan, P.J. Kilfoil, P. Haberzettl, B.G. Hill, S.P. Baba, L. Guo, K. Wetzelberger, D. Obal, D.G. Rokosh, R.A. Prough, S.D. Prabhu, M. Velayutham, J.L. Zweier, J.D. Hoetker, D.W. Riggs, S. Srivastava, R. Bolli, A. Bhatnagar, Genetic deficiency of glutathione S-transferase P increases myocardial sensitivity to Ischemia-Reperfusion Injury, Circ. Res. 117 (2015) 437–449.
[28] H. Ma, R. Guo, L. Yu, Y. Zhang, J. Ren, Aldehyde dehydrogenase 2 (ALDH2) rescues myocardial ischaemia/reperfusion injury: role of autophagy paradox and toxic aldehyde, Eur. Heart J. 32 (2011) 1025–1038.
[29] A. Sun, Y. Cheng, Y. Zhang, Q. Zhang, S. Wang, S. Tian, Y. Zou, K. Hu, J. Ren, J. Ge, Aldehyde dehydrogenase 2 ameliorates doxorubicin-induced myocardial dysfunction through detoxification of 4-HNE and suppression of autophagy, J. Mol. Cell. Cardiol. 71 (2014) 92–104.
[30] A. Divald, S.R. Powell, Proteasome mediates removal of proteins oxidized during myocardial ischemia, Free Radic. Biol. Med. 40 (2006) 156–164.
[31] S.R. Powell, P. Wang, H. Katzeff, R. Shringarpure, C. Teoh, I. Khaliulin, D.K. Das, K.J. Davies, H. Schwalb, Oxidized and ubiquitinated proteins may predict

recovery of postischemic cardiac function: essential role of the proteasome, Antioxid. Redox Signal. 7 (2005) 538–546.
[32] N.A. Strobel, R.G. Fassett, S.A. Marsh, J.S. Coombes, Oxidative stress biomarkers as predictors of cardiovascular disease, Int. J. Cardiol. 147 (2011) 191–201.
[33] V. Vemula, Z. Ni, M. Fedorova, Fluorescence labeling of carbonylated lipids and proteins in cells using coumarin-hydrazide, Redox Biol. 5 (2015) 195–204.
[34] C.A. Schneider, W.S. Rasband, K.W. Eliceiri, NIH image to ImageJ: 25 years of image analysis, Nat. Methods 9 (2012) 671–675.
[35] K. Bell, C. Wilding, S. Funke, N. Pfeiffer, F.H. Grus, Protective effect of 14-3-3 antibodies on stressed neuroretinal cells via the mitochondrial apoptosis pathway, BMC Ophthalmol. 15 (2015) 64.
[36] M.M. Bradford, A rapid and sensitive method for the quantitation of microgram quantities of protein utilizing the principle of protein-dye binding, Anal. Biochem. 72 (1976) 248–254.
[37] C.L. Ladner, J. Yang, R.J. Turner, R.A. Edwards, Visible fluorescent detection of proteins in polyacrylamide gels without staining, Anal. Biochem. 326 (2004) 13–20.
[38] B. Catalgol, B. Wendt, S. Grimm, N. Breusing, N.K. Ozer, T. Grune, Chromatin repair after oxidative stress: role of PARP-mediated proteasome activation, Free Radic. Biol. Med. 48 (2010) 673–680.
[39] T. Grune, B. Catalgol, A. Licht, G. Ermak, A.M. Pickering, J.K. Ngo, K.J. Davies, HSP70 mediates dissociation and reassociation of the 26S proteasome during adaptation to oxidative stress, Free Radic. Biol. Med. 51 (2011) 1355–1364.
[40] I. Milic, M. Fedorova, Derivatization and detection of small aliphatic and lipid-bound carbonylated lipid peroxidation products by ESI-MS, Methods Mol. Biol. 1208 (2015) 3–20.
[41] I. Milic, R. Hoffmann, M. Fedorova, Simultaneous detection of low and high molecular weight carbonylated compounds derived from lipid peroxidation by electrospray ionization-tandem mass spectrometry, Anal. Chem. 85 (2013) 156–162.
[42] Z. Ni, I. Milic, M. Fedorova, Identification of carbonylated lipids from different phospholipid classes by shotgun and LC-MS lipidomics, Anal. Bioanal. Chem. 407 (2015) 5161–5173.
[43] V. Matyash, G. Liebisch, T.V. Kurzchalia, A. Shevchenko, D. Schwudke, Lipid extraction by methyl-tert-butyl ether for high-throughput lipidomics, J. Lipid Res. 49 (2008) 1137–1146.
[44] R.C. Bollineni, M. Fedorova, M. Bluher, R. Hoffmann, Carbonylated plasma proteins as potential biomarkers of obesity induced type 2 diabetes mellitus, J. Proteome Res. 13 (2014) 5081–5093.
[45] D. Szklarczyk, A. Franceschini, S. Wyder, K. Forslund, D. Heller, J. Huerta-Cepas, M. Simonovic, A. Roth, A. Santos, K.P. Tsafou, M. Kuhn, P. Bork, L.J. Jensen, C. von Mering, STRING v10: protein-protein interaction networks, integrated over the tree of life, Nucleic Acids Res. 43 (2015) D447–452.
[46] I. Milic, E. Griesser, V. Vemula, N. Ieda, H. Nakagawa, N. Miyata, J.M. Galano, C. Oger, T. Durand, M. Fedorova, Profiling and relative quantification of multiply nitrated and oxidized fatty acids, Anal. Bioanal. Chem. (2015).
[47] S. Carballal, S. Bartesaghi, R. Radi, Kinetic and mechanistic considerations to assess the biological fate of peroxynitrite, Biochim. Et. Biophys. Acta 1840 (2014) 768–780.
[48] M.J. Kohr, H. Wang, D.G. Wheeler, M. Velayutham, J.L. Zweier, M.T. Ziolo, Biphasic effect of SIN-1 is reliant upon cardiomyocyte contractile state, Free Radic. Biol. Med. 45 (2008) 73–80.
[49] K. Konishi, N. Watanabe, T. Arai, SIN-1 cytotoxicity to PC12 cells is mediated by thiol-sensitive short-lived substances generated through SIN-1 decomposition in culture medium, Nitric Oxide : Biol. Chem. / Off. J. Nitric Oxide Soc. 20 (2009) 270–278.
[50] J.G. Dickhout, G.S. Hossain, L.M. Pozza, J. Zhou, S. Lhotak, R.C. Austin, Peroxynitrite causes endoplasmic reticulum stress and apoptosis in human vascular endothelium: implications in atherogenesis, Arterioscler. Thromb. Vasc. Biol. 25 (2005) 2623–2629.
[51] A. Schrammel, S. Pfeiffer, K. Schmidt, D. Koesling, B. Mayer, Activation of soluble guanylyl cyclase by the nitrovasodilator 3-morpholinosydnonimine involves formation of S-nitrosoglutathione, Mol. Pharmacol. 54 (1998) 207–212.
[52] I. Dalle-Donne, R. Rossi, R. Colombo, D. Giustarini, A. Milzani, Biomarkers of oxidative damage in human disease, Clin. Chem. 52 (2006) 601–623.
[53] S. Anavi, Z. Ni, O. Tirosh, M. Fedorova, Steatosis-induced proteins adducts with lipid peroxidation products and nuclear electrophilic stress in hepatocytes, Redox Biol. 4 (2015) 158–168.
[54] T. Jung, M. Engels, B. Kaiser, D. Poppek, T. Grune, Intracellular distribution of oxidized proteins and proteasome in HT22 cells during oxidative stress, Free Radic. Biol. Med. 40 (2006) 1303–1312.
[55] T. Jung, M. Engels, L.O. Klotz, K.D. Kroncke, T. Grune, Nitrotyrosine and protein carbonyls are equally distributed in HT22 cells after nitrosative stress, Free Radic. Biol. Med. 42 (2007) 773–786.
[56] K. Uchida, Lipid peroxidation and redox-sensitive signaling pathways, Curr. Atheroscler. Rep. 9 (2007) 216–221.
[57] K. Uchida, Role of reactive aldehyde in cardiovascular diseases, Free Radic. Biol. Med. 28 (2000) 1685–1696.
[58] M. Guichardant, M. Lagarde, Analysis of biomarkers from lipid peroxidation: a comparative study, Eur. J. Lipid Sci. Tech. 111 (2009) 75–82.
[59] E.K. Long, M.J. Picklo Sr., Trans-4-hydroxy-2-hexenal, a product of n-3 fatty acid peroxidation: make some room HNE, Free Radic. Biol. Med. 49 (2010) 1–8.
[60] M. Fedorova, R.C. Bollineni, R. Hoffmann, Protein carbonylation as a major hallmark of oxidative damage: update of analytical strategies, Mass Spectrom. Rev. 33 (2014) 79–97.
[61] M. Singh, A. Kapoor, A. Bhatnagar, Oxidative and reductive metabolism of lipid-peroxidation derived carbonyls, Chem. Biol. Inter. 234 (2015) 261–273.
[62] O. Yamaguchi, M. Taneike, K. Otsu, Cooperation between proteolytic systems in cardiomyocyte recycling, Cardiovasc. Res. 96 (2012) 46–52.
[63] R.A. Dunlop, U.T. Brunk, K.J. Rodgers, Oxidized proteins: mechanisms of removal and consequences of accumulation, IUBMB life 61 (2009) 522–527.
[64] G. Filomeni, D. De Zio, F. Cecconi, Oxidative stress and autophagy: the clash between damage and metabolic needs, Cell death Differ. 22 (2015) 377–388.
[65] Y. Mei, M.D. Thompson, R.A. Cohen, X. Tong, Autophagy and oxidative stress in cardiovascular diseases, Biochim. Et. Biophys. Acta 1852 (2015) 243–251.
[66] J. Yang, K.A. Tallman, N.A. Porter, D.C. Liebler, Quantitative chemoproteomics for site-specific analysis of protein alkylation by 4-hydroxy-2-nonenal in cells, Anal. Chem. 87 (2015) 2535–2541.
[67] A.F. Kisselev, A.L. Goldberg, Proteasome inhibitors: from research tools to drug candidates, Chem. Biol. 8 (2001) 739–758.
[68] K.G. Daniel, P. Gupta, R.H. Harbach, W.C. Guida, Q.P. Dou, Organic copper complexes as a new class of proteasome inhibitors and apoptosis inducers in human cancer cells, Biochem. Pharmacol. 67 (2004) 1139–1151.
[69] S. Tardito, A. Barilli, I. Bassanetti, M. Tegoni, O. Bussolati, R. Franchi-Gazzola, C. Mucchino, L. Marchio, Copper-dependent cytotoxicity of 8-hydroxyquinoline derivatives correlates with their hydrophobicity and does not require caspase activation, J. Med. Chem. 55 (2012) 10448–10459.
[70] M.J. Randall, M. Hristova, A. van der Vliet, Protein alkylation by the alpha,beta-unsaturated aldehyde acrolein. A reversible mechanism of electrophile signaling?, FEBS Lett. 587 (2013) 3808–3814.
[71] C. He, H. Zhu, W. Zhang, I. Okon, Q. Wang, H. Li, Y.Z. Le, Z. Xie, 7-Ketocholesterol induces autophagy in vascular smooth muscle cells through Nox4 and Atg4B, Am. J. Pathol. 183 (2013) 626–637.
[72] Y.C. Chang, M.C. Hsieh, H.J. Wu, W.C. Wu, Y.H. Kao, Methylglyoxal, a reactive glucose metabolite, enhances autophagy flux and suppresses proliferation of human retinal pigment epithelial ARPE-19 cells, Toxicol. Vitr. : Int. J. Publ. Assoc. BIBRA 29 (2015) 1358–1368.
[73] Y. Zhao, C.F. Zhang, H. Rossiter, L. Eckhart, U. Konig, S. Karner, M. Mildner, V.N. Bochkov, E. Tschachler, F. Gruber, Autophagy is induced by UVA and promotes removal of oxidized phospholipids and protein aggregates in epidermal keratinocytes, J. Invest. Dermatol. 133 (2013) 1629–1637.
[74] B.G. Hill, P. Haberzettl, Y. Ahmed, S. Srivastava, A. Bhatnagar, Unsaturated lipid peroxidation-derived aldehydes activate autophagy in vascular smooth-muscle cells, Biochem. J. 410 (2008) 525–534.
[75] P. Haberzettl, B.G. Hill, Oxidized lipids activate autophagy in a JNK-dependent manner by stimulating the endoplasmic reticulum stress response, Redox Biol. 1 (2013) 56–64.
[76] S.C. Kolwicz Jr., S. Purohit, R. Tian, Cardiac metabolism and its interactions with contraction, growth, and survival of cardiomyocytes, Circ. Res. 113 (2013) 603–616.
[77] I.J. Goldberg, C.M. Trent, P.C. Schulze, Lipid metabolism and toxicity in the heart, Cell Metab. 15 (2012) 805–812.
[78] A.R. Thiam, R.V. Farese Jr., T.C. Walther, The biophysics and cell biology of lipid droplets, Nat. Rev. Mol. Cell Biol. 14 (2013) 775–786.
[79] R. Singh, S. Kaushik, Y. Wang, Y. Xiang, I. Novak, M. Komatsu, K. Tanaka, A.M. Cuervo, M.J. Czaja, Autophagy regulates lipid metabolism, Nature 458 (2009) 1131–1135.
[80] R. Singh, A.M. Cuervo, Lipophagy: connecting autophagy and lipid metabolism, Int. J. Cell Biol. 2012 (2012) 282041.
[81] B. Jaishy, E.D. Abel, Lipids, lysosomes, and autophagy, J. Lipid Res. 57 (2016) 1619–1635.
[82] D. Mohammadyani, V.A. Tyurin, M. O'Brien, Y. Sadovsky, D.I. Gabrilovich, J. Klein-Seetharaman, V.E. Kagan, Molecular speciation and dynamics of oxidized triacylglycerols in lipid droplets: mass spectrometry and coarse-grained simulations, Free Radic. Biol. Med. 76 (2014) 53–60.
[83] G. Poli, F. Biasi, G. Leonarduzzi, 4-Hydroxynonenal-protein adducts: a reliable biomarker of lipid oxidation in liver diseases, Mol. Asp. Med. 29 (2008) 67–71.
[84] Q. Yuan, X. Zhu, L.M. Sayre, Chemical nature of stochastic generation of protein-based carbonyls: metal-catalyzed oxidation versus modification by products of lipid oxidation, Chem. Res. Toxicol. 20 (2007) 129–139.
[85] T.W. Lo, M.E. Westwood, A.C. McLellan, T. Selwood, P.J. Thornalley, Binding and modification of proteins by methylglyoxal under physiological conditions. A kinetic and mechanistic study with N alpha-acetylarginine, N alpha-acetylcysteine, and N alpha-acetyllysine, and bovine serum albumin, J. Biol. Chem. 269 (1994) 32299–32305.
[86] S. Mittelmaier, M. Pischetsrieder, Multistep ultrahigh performance liquid chromatography/tandem mass spectrometry analysis for untargeted quantification of glycating activity and identification of most relevant glycation products, Anal. Chem. 83 (2011) 9660–9668.
[87] J. Guo, K. Prokai-Tatrai, V. Nguyen, N. Rauniyar, B. Ughy, L. Prokai, Protein targets for carbonylation by 4-hydroxy-2-nonenal in rat liver mitochondria, J. Proteom. 74 (2011) 2370–2379.
[88] J.D. Chavez, J. Wu, W. Bisson, C.S. Maier, Site-specific proteomic analysis of lipoxidation adducts in cardiac mitochondria reveals chemical diversity of 2-alkenal adduction, J. Proteom. 74 (2011) 2417–2429.
[89] J. Wu, J.F. Stevens, C.S. Maier, Mass spectrometry-based quantification of myocardial protein adducts with acrolein in an in vivo model of oxidative stress, Mol. Nutr. Food Res. 55 (2011) 1401–1410.
[90] J.M. Chick, D. Kolippakkam, D.P. Nusinow, B. Zhai, R. Rad, E.L. Huttlin, S.P. Gygi, A mass-tolerant database search identifies a large proportion of unassigned spectra in shotgun proteomics as modified peptides, Nat. Biotechnol. 33 (2015) 743–749.

[91] E. Ahrne, F. Nikitin, F. Lisacek, M. Muller, QuickMod: a tool for open modification spectrum library searches, J. Proteome Res. 10 (2011) 2913–2921.
[92] D. Ye, Y. Fu, R.X. Sun, H.P. Wang, Z.F. Yuan, H. Chi, S.M. He, Open MS/MS spectral library search to identify unanticipated post-translational modifications and increase spectral identification rate, Bioinformatics 26 (2010) i399–406.
[93] C.W. Ma, H. Lam, Hunting for unexpected post-translational modifications by spectral library searching with tier-wise scoring, J. Proteome Res. 13 (2014) 2262–2271.
[94] B. Fogelgren, N. Polgar, K.M. Szauter, Z. Ujfaludi, R. Laczko, K.S. Fong, K. Csiszar, Cellular fibronectin binds to lysyl oxidase with high affinity and is critical for its proteolytic activation, J. Biol. Chem. 280 (2005) 24690–24697.
[95] I.M. Moller, A. Rogowska-Wrzesinska, R.S. Rao, Protein carbonylation and metal-catalyzed protein oxidation in a cellular perspective, J. Proteom. 74 (2011) 2228–2242.
[96] R.C. Bollineni, R. Hoffmann, M. Fedorova, Proteome-wide profiling of carbonylated proteins and carbonylation sites in HeLa cells under mild oxidative stress conditions, Free Radic. Biol. Med. 68 (2014) 186–195.
[97] R.M. LoPachin, T. Gavin, Molecular mechanisms of aldehyde toxicity: a chemical perspective, Chem. Res. Toxicol. 27 (2014) 1081–1091.
[98] Y.V. Vasil'ev, S.C. Tzeng, L. Huang, C.S. Maier, Protein modifications by electrophilic lipoxidation products: adduct formation, chemical strategies and tandem mass spectrometry for their detection and identification, Mass Spectrom. Rev. 33 (2014) 157–182.
[99] A. Annibal, K. Schubert, U. Wagner, R. Hoffmann, J. Schiller, M. Fedorova, New covalent modifications of phosphatidylethanolamine by alkanals: mass spectrometry based structural characterization and biological effects, J. Mass Spectrom. : JMS 49 (2014) 557–569.
[100] B. Aryal, J. Jeong, V.A. Rao, Doxorubicin-induced carbonylation and degradation of cardiac myosin binding protein C promote cardiotoxicity, Proc. Natl. Acad. Sci. U.S.A. 111 (2014) 2011–2016.
[101] M. Beck, A. Schmidt, J. Malmstroem, M. Claassen, A. Ori, A. Szymborska, F. Herzog, O. Rinner, J. Ellenberg, R. Aebersold, The quantitative proteome of a human cell line, Mol. Syst. Biol. 7 (2011) 549.
[102] E. Cabiscol, J. Tamarit, J. Ros, Protein carbonylation: proteomics, specificity and relevance to aging, Mass Spectrom. Rev. 33 (2014) 21–48.
[103] P.A. Grimsrud, M.J. Picklo Sr., T.J. Griffin, D.A. Bernlohr, Carbonylation of adipose proteins in obesity and insulin resistance: identification of adipocyte fatty acid-binding protein as a cellular target of 4-hydroxynonenal, Mol. Cell. Proteom. : MCP 6 (2007) 624–637.
[104] D.L. Meany, H. Xie, L.V. Thompson, E.A. Arriaga, T.J. Griffin, Identification of carbonylated proteins from enriched rat skeletal muscle mitochondria using affinity chromatography-stable isotope labeling and tandem mass spectrometry, Proteomics 7 (2007) 1150–1163.
[105] J. Feng, H. Xie, D.L. Meany, L.V. Thompson, E.A. Arriaga, T.J. Griffin, Quantitative proteomic profiling of muscle type-dependent and age-dependent protein carbonylation in rat skeletal muscle mitochondria. *The journals of gerontology*, Ser. A, Biol. Sci. Med. Sci. 63 (2008) 1137–1152.
[106] Y. Zhao, S. Miriyala, L. Miao, M. Mitov, D. Schnell, S.K. Dhar, J. Cai, J.B. Klein, R. Sultana, D.A. Butterfield, M. Vore, I. Batinic-Haberle, S. Bondada, D.K. St Clair, Redox proteomic identification of HNE-bound mitochondrial proteins in cardiac tissues reveals a systemic effect on energy metabolism after doxorubicin treatment, Free Radic. Biol. Med. 72 (2014) 55–65.
[107] J. Chen, S. Schenker, T.A. Frosto, G.I. Henderson, Inhibition of cytochrome c oxidase activity by 4-hydroxynonenal (HNE). role of HNE adduct formation with the enzyme subunits, Biochim. Et. Biophys. Acta 1380 (1998) 336–344.
[108] J.H. Yang, E.S. Yang, J.W. Park, Inactivation of NADP+-dependent isocitrate dehydrogenase by lipid peroxidation products, Free Radic. Res. 38 (2004) 241–249.
[109] J.J. Galligan, K.L. Rose, W.N. Beavers, S. Hill, K.A. Tallman, W.P. Tansey, L.J. Marnett, Stable histone adduction by 4-oxo-2-nonenal: a potential link between oxidative stress and epigenetics, J. Am. Chem. Soc. 136 (2014) 11864–11866.
[110] E. Augustyniak, A. Adam, K. Wojdyla, A. Rogowska-Wrzesinska, R. Willetts, A. Korkmaz, M. Atalay, D. Weber, T. Grune, C. Borsa, D. Gradinaru, R. Chand Bollineni, M. Fedorova, H.R. Griffiths, Validation of protein carbonyl measurement: a multi-centre study, Redox Biol. 4 (2015) 149–157.
[111] E. Niggli, N.D. Ullrich, D. Gutierrez, S. Kyrychenko, E. Polakova, N. Shirokova, Posttranslational modifications of cardiac ryanodine receptors: Ca(2+) signaling and EC-coupling, Biochim. Et. Biophys. Acta 1833 (2013) 866–875.
[112] C.M. Sag, S. Wagner, L.S. Maier, Role of oxidants on calcium and sodium movement in healthy and diseased cardiac myocytes, Free Radic. Biol. Med. 63 (2013) 338–349.
[113] L. Xu, J.P. Eu, G. Meissner, J.S. Stamler, Activation of the cardiac calcium release channel (ryanodine receptor) by poly-S-nitrosylation, Science 279 (1998) 234–237.
[114] D.R. Gonzalez, A.V. Treuer, J. Castellanos, R.A. Dulce, J.M. Hare, Impaired S-nitrosylation of the ryanodine receptor caused by xanthine oxidase activity contributes to calcium leak in heart failure, J. Biol. Chem. 285 (2010) 28938–28945.
[115] L.L. Cooper, W. Li, Y. Lu, J. Centracchio, R. Terentyeva, G. Koren, D. Terentyev, Redox modification of ryanodine receptors by mitochondria-derived reactive oxygen species contributes to aberrant Ca2+ handling in ageing rabbit hearts, J. Physiol. 591 (2013) 5895–5911.
[116] V.P. Johnstone, L.C. Hool, Glutathionylation of the L-type Ca2+ channel in oxidative stress-induced pathology of the heart, Int. J. Mol. Sci. 15 (2014) 19203–19225.
[117] J. Cai, J. Chen, H. He, Z. Yin, Z. Zhu, D. Yin, Carbonyl stress: malondialdehyde induces damage on rat hippocampal neurons by disturbance of Ca(2+) homeostasis, Cell Biol. Toxicol. 25 (2009) 435–445.
[118] B.M. Radu, D.I. Dumitrescu, C.C. Mustaciosu, M. Radu, Dual effect of methylglyoxal on the intracellular Ca2+ signaling and neurite outgrowth in mouse sensory neurons, Cell. Mol. Neurobiol. 32 (2012) 1047–1057.
[119] E. Albano, G. Bellomo, M. Parola, R. Carini, M.U. Dianzani, Stimulation of lipid peroxidation increases the intracellular calcium content of isolated hepatocytes, Biochim. Et. Biophys. Acta 1091 (1991) 310–316.
[120] C. Lu, S.L. Chan, W. Fu, M.P. Mattson, The lipid peroxidation product 4-hydroxynonenal facilitates opening of voltage-dependent Ca2+ channels in neurons by increasing protein tyrosine phosphorylation, J. Biol. Chem. 277 (2002) 24368–24375.
[121] C.H. Shao, C. Tian, S. Ouyang, C.J. Moore, F. Alomar, I. Nemet, A. D'Souza, R. Nagai, S. Kutty, G.J. Rozanski, S. Ramanadham, J. Singh, K.R. Bidasee, Carbonylation induces heterogeneity in cardiac ryanodine receptor function in diabetes mellitus, Mol. Pharmacol. 82 (2012) 383–399.